

2018

## MEASUREMENTS OF MODAL ATTENUATION USING BROADBAND SOURCES IN THE NEW ENGLAND MUD PATCH

Kerry Unrein  
*University of Rhode Island, kerrcut@gmail.com*

Follow this and additional works at: <https://digitalcommons.uri.edu/theses>

Terms of Use

All rights reserved under copyright.

---

### Recommended Citation

Unrein, Kerry, "MEASUREMENTS OF MODAL ATTENUATION USING BROADBAND SOURCES IN THE NEW ENGLAND MUD PATCH" (2018). *Open Access Master's Theses*. Paper 1426.  
<https://digitalcommons.uri.edu/theses/1426>

This Thesis is brought to you by the University of Rhode Island. It has been accepted for inclusion in Open Access Master's Theses by an authorized administrator of DigitalCommons@URI. For more information, please contact [digitalcommons-group@uri.edu](mailto:digitalcommons-group@uri.edu). For permission to reuse copyrighted content, contact the author directly.

MEASUREMENTS OF MODAL ATTENUATION USING BROADBAND SOURCES  
IN THE NEW ENGLAND MUD PATCH

BY

KERRY UNREIN

A THESIS SUBMITTED IN FULFILLMENT OF THE REQUIREMENTS FOR THE  
DEGREE OF MASTER OF SCIENCE

IN

OCEAN ENGINEERING

UNIVERSITY OF RHODE ISLAND

2018

DEGREE OF MASTER OF SCIENCE THESIS  
OF  
KERRY UNREIN

APPROVED:

Thesis Committee:

Co-Major Professor Gopu R. Potty

Co-Major Professor James H. Miller

Lora J. Van Uffelen

Aaron S. Bradshaw

Nasser H. Zawia  
DEAN OF THE GRADUATE SCHOOL

UNIVERSITY OF RHODE ISLAND  
2018

## ABSTRACT

Measurements of underwater acoustic signals were made on a bottom-mounted horizontal line array during the Seabed Characterization Experiment (SBCEX) in the New England Mud Patch south of Martha's Vineyard in about 70 m of water. The signals were generated by Signals, Underwater Sound (SUS) charges detonated at various locations in the experimental area at a depth of 18 m, during nearly-isovelocity conditions. The broadband signals were analyzed for modal arrival time and amplitude using time-frequency techniques. Ratios of modal amplitudes at the individual hydrophones were used to estimate the modal attenuation coefficients. Hence, these estimates are independent of any uncertainty in the frequency-dependent source level of the SUS charges. These coefficients are directly related to the depth-dependent sediment attenuation profile. Posteriori error analysis provides averages and standard deviations for the estimate of sediment attenuation as function of depth. The frequency bands of interest range from 30 Hz to 120 Hz for modes one through four. We compared our estimates of sediment attenuation with historical measurements. We determined the frequency exponent of mud to be 1.9 with an attenuation coefficient on the order of  $10^{-5}$  to  $10^{-4}$  decibels per meter. This work was supported by the Office of Naval Research.

## ACKNOWLEDGMENTS

I would like to thank my thesis advisors, Dr. Gopu R. Potty and Dr. James H. Miller for their guidance and willingness to share their wealth of expertise on the subject matter with me. Their unwavering support and genuine enthusiasm for acoustics kept me motivated and looking forward to class through the years. I have much gratitude to Dr. Lora Van Uffelen, Dr. Aaron Bradshaw, and the defense chair Dr. Arthur Spivack for their feedback and comments as part of the thesis committee at the University of Rhode Island.

Thank you to the Office of Naval Research for the opportunity to work on a fascinating topic in acoustics. Thank you to Dag Tollefsen of the Norwegian Defense Research Establishment, Horten, Norway for providing the data for research. Thank you to David Knobles of KSA, Preston Wilson of the Mechanical Engineering and Applied Research Laboratories at the University of Texas at Austin, and Ying-Tsong Lin from Applied Ocean Physics and Engineering of the Woods Hole Oceanographic Institution for sharing their research from the Seabed Characterization Experiment.

Thank you to my husband for his support and patience. I would not have made it through without you.

# TABLE OF CONTENTS

<b>ABSTRACT .....</b>	<b>ii</b>
<b>ACKNOWLEDGMENTS .....</b>	<b>iii</b>
<b>TABLE OF CONTENTS.....</b>	<b>iv</b>
<b>LIST OF TABLES .....</b>	<b>vi</b>
<b>LIST OF FIGURES .....</b>	<b>vii</b>
<b>1 INTRODUCTION.....</b>	<b>1</b>
1.1 Background .....	1
1.2 Thesis Overview .....	3
<b>2 BACKGROUND .....</b>	<b>5</b>
2.1 Attenuation Derived from Sediment Properties .....	5
2.2 Normal Mode Theory .....	7
2.3 Computation of Mode Travel Time Dispersion.....	11
2.4 Overview of Genetic Algorithm .....	12
2.5 A Posteriori Analysis .....	15
<b>3 EXPERIMENT DESCRIPTION.....</b>	<b>16</b>
3.1 Site Description.....	16
3.2 Signals, Underwater Sound (SUS) Description.....	17
3.3 Horizontal Line Array Description.....	18
3.4 Environmental Conditions .....	19
<b>4 METHODOLOGY.....</b>	<b>23</b>
4.1 Data Selection .....	23
4.2 Data Processing Overview .....	25
4.3 Time-Frequency Analysis for Modal Amplitude Selection.....	27
4.3 Calculation of Experimental Modal Amplitude Ratios.....	31

4.4 Parameter Descriptions for Genetic Algorithm Computation .....	31
4.5 Calculation of Theoretical Modal Amplitude Ratios.....	33
4.6 Error Minimization.....	34
<b>5 RESULTS .....</b>	<b>36</b>
5.1 A Posteriori Analysis of Depth Dependent Attenuation .....	36
5.2 Range Verification.....	40
5.3 Comparison to Historic Data.....	42
5.4 Sensitivity Analysis.....	44
<b>6 CONCLUSION.....</b>	<b>45</b>
<b>APPENDICES .....</b>	<b>46</b>
Appendix A. Field Log Excerpt for SUS Charge Recordings.....	46
Appendix B. MATLAB Code .....	48
Appendix C. Attenuation Coefficient by Depth for Station 49 .....	79
<b>BIBLIOGRAPHY .....</b>	<b>81</b>

## LIST OF TABLES

TABLE	PAGE
Table 1. Biot-Stoll input sediment parameters for compressional wave attenuation modeling (Badiey, 1998).....	6
Table 2. SUS stations listed by deployment date and coordinate. ....	23
Table 3. The table lists amplitude in decibels of modes one through four, calculated for each hydrophone during the fifth SUS detonation at Station 49. ....	30
Table 4. Thirteen parameters were optimized by the genetic algorithm.....	32
Table 5. Summary of <i>a posteriori</i> statistical analysis for each parameter on all SUS for Stations 49 and 54. ....	36

## LIST OF FIGURES

FIGURE	PAGE
Figure 1. Attenuation coefficients plotted as a function of frequency for seawater (A') and fresh water (B'). The frequency range examined in this experiment is circled in red (Jensen et al., 1994).....	3
Figure 2. The first four normal modes in an ideal waveguide of depth 100 meters. (Jensen et al., 1994).....	9
Figure 3. The wave envelope $V_g$ , outlines group velocity propagation and $v_m$ , is the phase velocity (Frisk, 1994).....	10
Figure 4. Dispersion curves of modes one through three in an ideal waveguide.....	10
Figure 5. Flow diagram of genetic algorithm optimization (Potty et al., 2000). ....	13
Figure 6. Illustration of crossover between generations during optimization (Tang et al., 1996 ). ....	13
Figure 7. Above, the binary encoding of the parameters for each generation is shown with mutated parameters indicated by a one (Tang et al., 1996 ). ....	14
Figure 8. Complete net topology with unrestricted migration during genetic algorithm selection (Tang et al., 1996).....	14
Figure 9. The experiment location is outlined in blue. The color map indicates grain size obtained by survey techniques prior to the experiment (Goff et al., 2018). ....	17
Figure 10. Above is an overhead view of the experimental site. The horizontal line array is positioned to the northeast marked as FFI HLA. The SUS charges deployed are depicted by green circles in a radial pattern (Knobles et al., 2019). ....	18
Figure 11. Cross section of the experiment setup. ....	19
Figure 12. Hydrophones examined on the bottom-mounted horizontal line array. ....	19
Figure 13. New England Mud Patch sound speed and density profiles obtained by inversion (Bonnell et al., 2018).....	21
Figure 14. The density profile and thickness for the New England Mud Patch sediment boundary layer is shown above. The image is not to scale (Goff et al., 2018). ....	22

FIGURE	PAGE
Figure 15. Map of array and SUS charges color-coded to the day of deployment. ....	24
Figure 16. Above, the difference in time of arrival is plotted for the different hydrophones. The hydrophone number is noted to the right. ....	25
Figure 17. Data flow of parameter optimization using genetic algorithms as developed by Potty et al. in “Inversion for sediment geoaoustic properties at the New England Bight” (2003). ....	26
Figure 18. Scalogram of the fifth and last SUS charge deployed at Station 49. ....	28
Figure 19. Scalogram of the fifth and last SUS deployed at Station 49, which is the same image as Figure 18. The white dotted lines note the time-frequency slices what were examined for amplitude selection. ....	28
Figure 20. Time series at the frequency slice 32.1 Hz from the fifth and last SUS at Station 49 is shown. The upper image depicts the time-frequency slice, while the lower image utilized a third octave filter demodulate of the same signal. ....	29
Figure 21. Above are the genetic algorithm lowest misfit parameters and standard deviation for each layer. The mud layer is expanded in the red box. ....	38
Figure 22. Above is the <i>a posteriori</i> average of the 50 lowest misfit parameters for each layer and standard deviation. The mud layer is expanded in the red box. ....	38
Figure 23. Above are the genetic algorithm best output parameters demonstrating attenuation dependence on frequency. The mud layer is expanded in the red box. ....	39
Figure 24. Above are the <i>a posteriori</i> average output parameters demonstrating attenuation dependence on frequency. The mud layer is expanded in the red box. ....	39
Figure 25. To the left, time of arrival and frequency are selected by peak modal amplitude from the experimental data. To the right, theoretical group velocity difference by mode on the x-axis is compared to experimental travel time difference on the y-axis. Data is from the first SUS charge deployed at Station 49 approximately 8 km away from hydrophone one on the array. ....	40
Figure 26. To the left, time of arrival and frequency are selected by peak modal amplitude from the experimental data. To the right, theoretical group velocity difference by mode on the x-axis is compared to experimental travel time difference on the y-axis. Data is for the first SUS charge deployed at Station 54 approximately 13 km away from hydrophone one on the array. ....	41

FIGURE

PAGE

Figure 27. SBCEX average attenuation coefficient  $\alpha(z)$  for Station 49 and 54 overlaid published experimental results. The seafloor surface mud layer is shown in cyan and the deep layer one is in magenta (Zhou et al., 2009). ..... 43

Figure 28. This plot examines the sensitivity of attenuation as a function of depth. A 10% perturbation of attenuation was applied at various depths (Potty et al., 2018).... 44

# CHAPTER 1

## INTRODUCTION

### *1.1 Background*

Acoustic propagation through the ocean is influenced by many environmental factors including interaction with the seafloor. Since it is difficult to obtain samples to verify the precise composition of the seabed, acoustic methods are of interest for characterizing the seafloor. Inverse methods are utilized in this study to estimate effective modal attenuation coefficients derived from data collected at hydrophones on a horizontal line array (HLA). We compare these attenuation coefficients to published historical data.

Similar analyses were conducted in 1999 and 2002 to infer sediment attenuation properties based on broadband source effects on vertical line arrays (VLAs) (Potty et al., 1999 and 2002). They estimated bottom attenuation coefficients based on modal amplitude ratios using SUS data from a single hydrophone. The use of amplitude ratios eliminates the need to know the exact source level of Signals, Underwater Sound (SUS) charges. Genetic algorithms were used to optimize the search parameters including sound wave speed through sediment. The inversions compared well to core data collected in the experimental area giving confidence in the method. Lastly, a sensitivity study was conducted to evaluate the uncertainty in the parameter contribution to the results.

Attenuation is a reduction of sound intensity as an acoustic wave propagates in range. As the sound wave propagates through a medium, some of its energy is

converted into heat. This frequency dependent effect is called sound attenuation or absorption. Other factors such as scattering along interfaces and within the volume can cause additional losses. Most acoustic inversion methods estimate the total losses (effective attenuation).

For comparison purposes, the attenuation of seawater must be considered. The attenuation of seawater is also frequency dependent and important for evaluating the feasibility of sediment attenuation coefficients for this experiment. The equation for the attenuation of water is (Jensen et al., 1994)

$$\alpha \approx 3.3 \times 10^{-3} + \frac{0.11f^2}{1 + f^2} + \frac{44f^2}{4100 + f^2} + 3.0 \times 10^{-4}f^2 \left[ \frac{dB}{km} \right]. \quad (1.1)$$

A plot of this equation from Jensen et al. (1994) is displayed in Figure 1. We studied lower frequencies, indicated by the red circle on the plot. The surface sediment attenuation coefficient is expected to be higher than 0.00002 dB/m of seawater at ten degrees Celsius (Ainslie, 1998).

Mud at the water and sediment interface boundary is thought to have an attenuation coefficient between sand and seawater (Pierce, 2015). This thesis investigates the attenuation coefficient of the mud layer of the New England Mud Patch from an experiment conducted in March 2017.

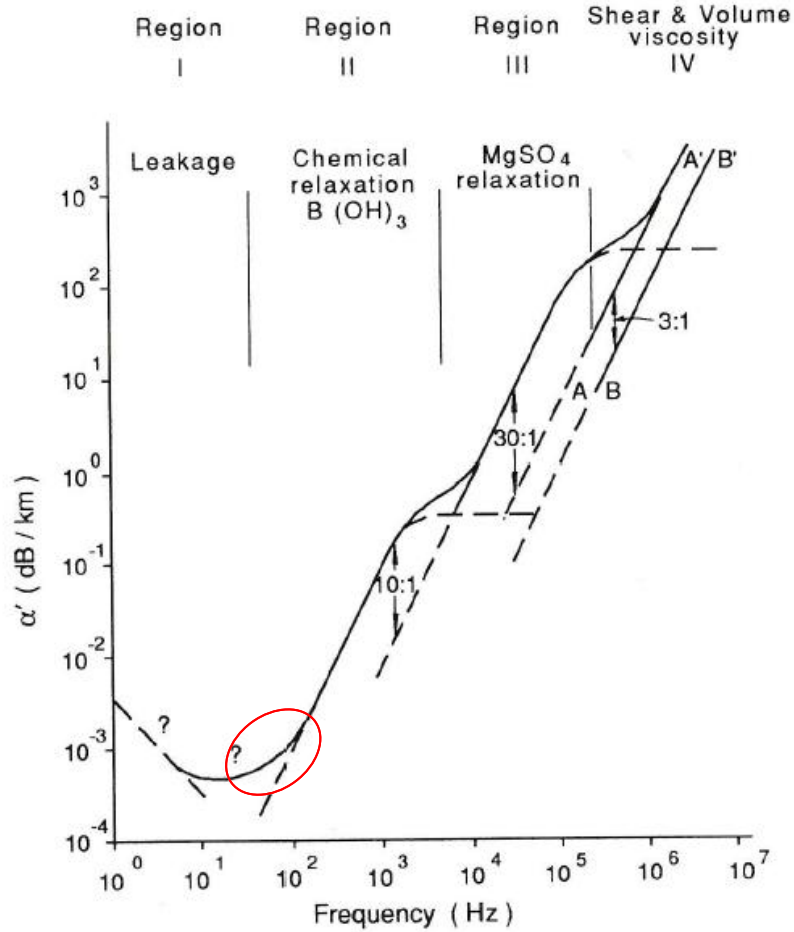


Figure 1. Attenuation coefficients plotted as a function of frequency for seawater (A') and fresh water (B'). The frequency range examined in this experiment is circled in red (Jensen et al., 1994).

### 1.2 Thesis Overview

This thesis consists of six chapters. Chapter 2 describes the equations and theories that are the basis of the analysis. There is a brief description of two sediment material property theories for computing intrinsic attenuation. Intrinsic attenuation is the attenuation related to damping from sediment mechanics, where effective attenuation is the overall sound reduction of a source in an environment. Normal mode theory is described in detail with a derivation for acoustic pressure. There is a section

describing a way to compute the separation between source and receiver using group velocity developed by Potty et al. (2003). Genetic algorithms and their applications to optimization are introduced. Lastly, the equations for analysis *a posteriori* on the genetic algorithm output are presented.

Chapter 3 gives an overview of the Seabed Characterization Experiment (SBCEX) and the equipment relevant to this thesis. The environmental conditions and site composition are described.

Chapter 4 details the analysis performed using the theories from Chapter 2. A flow diagram incorporating the variables and equations of the attenuation computation is available in Figure 17 to highlight the optimization steps.

Chapter 5 presents the estimated parameters and resulting attenuation as a function of depth in tabular and graphical form. The attenuation coefficients as a function of frequency are directly compared to previous work on sandy sea bottoms.

## CHAPTER 2

### BACKGROUND

#### *2.1 Attenuation Derived from Sediment Properties*

Intrinsic attenuation is derived from sediment properties. This attenuation describes the damping of sound waves due to friction. Sound vibrates the grains and trapped water throughout marine sediments, resulting in a reduction of intensity.

There are a number of geoacoustic models available for deriving seabed acoustic properties from direct sediment measurement of physical parameters. One of the widely used models is the Biot-Stoll model. Biot deduced equations for modeling poroelastic properties as a “granular solid forming a porous skeleton, which is filled with fluid” (Badiy, 1998). Stoll specifically applied these properties to the seafloor to predict frequency-dependent attenuation. Because the voids in the sea floor sediment layers are interconnected, there is greater observed attenuation resulting from “not only intergranular friction, but also the additional losses owing to the viscosity of the fluid.” The intergranular frame squeezes the local fluid, causing damping, resulting in frequency dependence (Stoll, 1985). The Biot-Stoll model takes into account thirteen different parameters to compute intrinsic attenuation. The parameters are listed in Table 1 (Badiy, 1998). The compressional wave attenuation of low frequencies for ‘highly permeable sediment’ was found to increase at  $f^2$ , where  $f$  is the frequency in Hz (Buchanan, 2005).

The parameters for the Biot-Stoll model are listed in Table 1 (Badiy, 1998).

Table 1. Biot-Stoll input sediment parameters for compressional wave attenuation modeling (Badiey, 1998).

Parameter	Symbol	Unit
Grain density	$\rho_s$	kg/m <sup>3</sup>
Fluid density	$\rho_f$	kg/m <sup>3</sup>
Grain bulk modulus	$K_s$	Pa
Fluid bulk modulus	$K_f$	Pa
Frame bulk modulus	$K_0$	Pa
Frame shear modulus	$G_0$	Pa
Fluid viscosity	$\mu_f$	kg/m·s
Permeability	k	m <sup>2</sup>
Porosity	$\phi$	n/a
Degree of saturation	S	n/a
Shear specific loss	$\delta'$	n/a
Volumetric specific loss	$\delta''$	n/a
Added mass coefficient	c	n/a

Another popular model was developed by Michael Buckingham some years later. He identified a relationship of  $f^1$  for a frequency range from 1 Hz to 1 MHz for frequency dependent attenuation (Buchanan, 2005). He reported attenuation to be much more dependent on the “intergranular dissipation” between grains, loosely calling it “friction” for simplicity. The marine sediment is treated as a bulk fluid, not as the frame Stoll suggested. Particle size, roughness, and packing ability are the driving factors in addition to porosity and density that contribute to the attenuation of surface sediments. Consequently, the Buckingham model requires significantly fewer parameters than the Biot-Stoll model (Buckingham, 1997).

While these theories are not directly implemented in this thesis, the background provides a broader understanding of attenuation.

## 2.2 Normal Mode Theory

Let's start with the acoustic wave equation (Urlick, 1983).

$$\frac{\partial^2 p}{\partial t^2} = c^2 \left( \frac{\partial^2 p}{\partial x^2} + \frac{\partial^2 p}{\partial y^2} + \frac{\partial^2 p}{\partial z^2} \right) \quad (2.1)$$

Converting to cylindrical coordinates to represent spreading from a point source in a waveguide, the solution to the wave equation is the following inhomogeneous Helmholtz equation. Symmetrical cylindrical spreading is assumed about the z-axis, so the wave equation no longer requires solving for  $\theta$  (Jensen, 1994).

$$\frac{1}{r} \frac{\partial}{\partial r} \left[ r \frac{\partial p(r, z)}{\partial r} \right] + \rho(z) \frac{\partial}{\partial z} \left[ \frac{1}{\rho(z)} \right] \frac{\partial p(r, z)}{\partial z} + k^2(z) p(r, z) = -\frac{\delta(r) \delta(z - z_s)}{2\pi r} \quad (2.2)$$

Harmonic time-dependence  $e^{-i\omega t}$  is assumed for ambient environment pressure  $p(r, z)$ .

The point source is represented by the Dirac delta function  $\delta$ , triggered in a horizontally stratified water column of separation  $r$  from the receiver. Density  $\rho(z)$  and sound speed  $c(z)$  are a function of depth  $z$ . The variable  $k$  is the wave number in rad/m, similar to spatial frequency, and is equal to  $\frac{\omega}{c(z)}$ .

A solution is obtained using the separation of variables technique. The equation is broken into a solution for depth and a solution for range. The variable  $p(r, z)$  is solved in the form  $p(r, z) = \phi(r)\psi(z)$ . The solution is unforced and therefore equal to zero.

$$\frac{1}{\phi} \left[ \frac{1}{r} \frac{\partial}{\partial r} \left( r \frac{\partial \phi}{\partial r} \right) \right] + \frac{1}{\psi} \left[ \rho(z) \frac{\partial}{\partial z} \left( \frac{1}{\rho(z)} \frac{\partial \psi}{\partial z} \right) + k^2(z) \psi \right] = 0 \quad (2.3)$$

The range term  $\phi$  is to the left of the plus sign and the depth term  $\psi$  is to the right in Eq. 2.3.

The depth equation is solved as a Sturm-Liouville problem as outlined by Jensen et al. (1994) to obtain the eigenfunctions to solve for  $\psi$ .

$$\rho(z) \frac{\partial}{\partial z} \left( \frac{1}{\rho(z)} \frac{\partial \psi_m(z)}{\partial z} \right) + [k^2(z) - \kappa_{rm}^2] \psi_m(z) = 0 \quad (2.4)$$

Please note the addition of the  $\kappa_{rm}$  term and change of  $\psi(z)$  to  $\psi_m(z)$ . This reflects the variability of the separation constant in the modal equation required to follow the Sturm-Liouville problem. The variable  $\psi_m(z)$  is an eigenfunction and describes mode shape. The modes must be orthogonal.  $\kappa_{rm}$  is an eigenvalue that is the horizontal propagation constant, similar to frequency of vibration. The  $\kappa_{rm}$  values are sorted in descending order and must be discrete, real, and positive. The modes form a summation that is used to solve for pressure.

The following is the range portion of the separated variable equation.

$$\frac{1}{r} \frac{\partial}{\partial r} \left[ r \frac{\partial \phi_n(r)}{\partial r} \right] + \kappa_n^2 \phi_n(r) = 0 \quad (2.5)$$

The solution for  $\phi_n$  is the Hankel function of the first kind (Jensen et al., 1994).

$$\phi_n(r) = H_0^{(1)}(k_n r) \quad (2.6)$$

$$\text{where } H_0^{(1)} k r \simeq \sqrt{\frac{2}{\pi k r}} e^{i(kr - \pi/4)}.$$

This form the Hankel function is intended for use as  $kr \rightarrow \infty$  and more than a wavelength  $\lambda$  away. The wavelength equation is  $\lambda = \frac{c}{f}$ , where  $c$  is nominally 1500 m/s and frequency  $f$  ranges from 20 to 120 Hz. Any separation greater than 75 m is greater than a wavelength away from the source (Jensen et al., 1994).

The solution for pressure is a set of modes.

$$p(r, z) = \sum_{m=1}^{\infty} \phi_m(r) \psi_m(z) \quad (2.7)$$

The resulting modal pressure is the following equation (Potty et al., 2003).

$$p_m(r, z) \approx \frac{e^{-\frac{i\pi}{4}}}{\rho(z_s) \sqrt{8\pi r}} \sum_{m=1}^M \psi_m(z_s) \psi_m(z) \frac{e^{ik_m r}}{\sqrt{k_{rm}}} e^{-\beta_m r} \quad (2.8)$$

This pressure computation is used in Chapter 4 for computation of the theoretical pressure resulting from the optimized parameters of the genetic inversion.

In an ideal stratified waveguide with constant sound speed and density, perfectly reflecting pressure relief surface and perfectly reflecting hard bottom, the modes are sine waves. The first four modes in a 100 m deep ideal waveguide are shown in Figure 2.

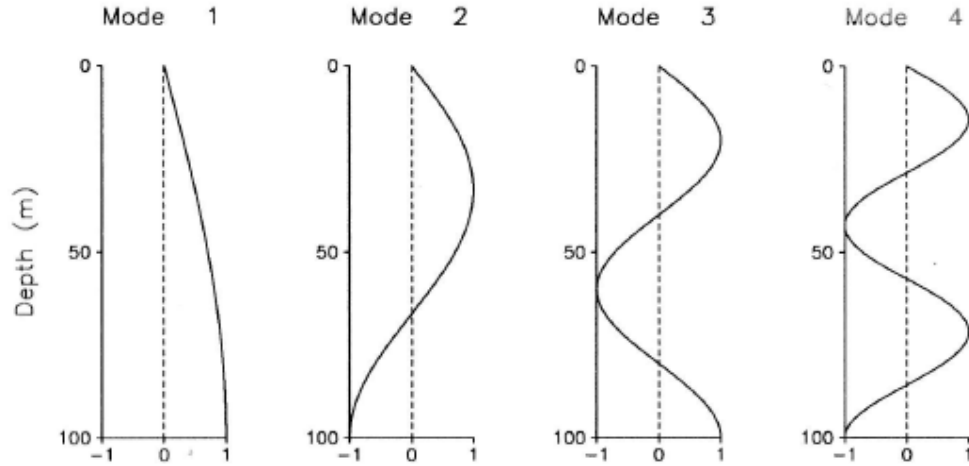


Figure 2. The first four normal modes in an ideal waveguide of depth 100 meters. (Jensen et al., 1994).

Dispersion is the effect of phase velocity separation due to the frequency dependence of wave velocity and is only relevant to broadband sources. Each mode has a unique phase or wave front velocity. Phase velocity  $v_m$ , is a function of angular frequency and is the ratio of frequency to the wave number of the mode

$$v_m(\omega) = \frac{\omega}{k_m} \quad (2.9)$$

where  $\omega = 2\pi f$ ,  $k_m$  is the wave number, and  $m$  is the mode number (Frisk, 1994).

Phase velocity is the speed at which the phase front of a wave propagates and group velocity is the speed at which energy travels. Group velocity can be represented as the speed at which the envelope will move as shown in Figure 3.

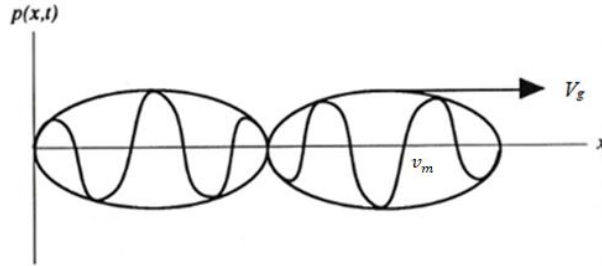


Figure 3. The wave envelope  $V_g$ , outlines group velocity propagation and  $v_m$ , is the phase velocity (Frisk, 1994).

Group velocity is related to phase velocity by

$$V_g = \frac{d\omega}{dk_m} = \frac{d(v_m k_m)}{dk_m} = v_m + k_m \frac{dv_m}{dk_m}. \quad (2.10)$$

Group velocity will always be less than the sound speed, where phase velocity is always faster (Frisk, 1994). This is shown in Figure 4 depicting dispersion curves of an ideal waveguide.

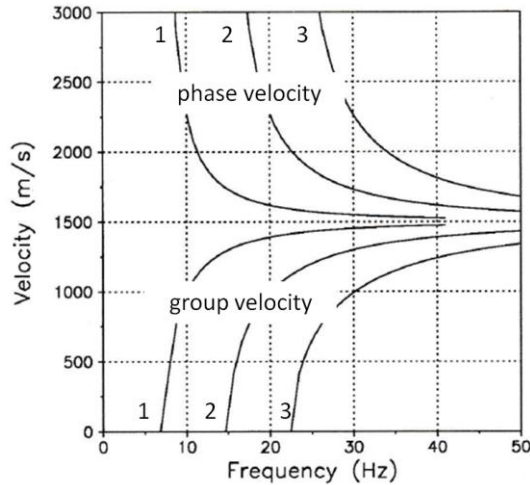


Figure 4. Dispersion curves of modes one through three in an ideal waveguide

(Jensen et al., 1994).

Modal attenuation can be found as a function of the intrinsic attenuation (Rajan et al., 1987).

$$\beta_m = \frac{\int_0^\infty \alpha(z)k(z)|\psi_m(z)|^2 dz}{\kappa_m} \quad (2.11)$$

$\beta_m$  is the modal attenuation coefficient of mode  $m$ ,  $\alpha(z)$  is attenuation as a function of depth,  $k(z)$  is the wave number of the profile  $\frac{2\pi f}{c(z)}$  also as a function of depth,  $\psi_m$  is the mode shape, and  $\kappa_m$  is the modal horizontal propagation constant (Rajan, 1987).

### 2.3 Computation of Mode Travel Time Dispersion

The source-receiver range is computed using the modal travel time between the individual modes. This data is calculated from the time-frequency diagram of the broadband SUS data. Based on the group velocities calculated using Eq. 2.10, the modal travel time differences can also be predicted based on the assumed geoacoustic model. Using the observed and predicted modal travel time differences, the source-receiver range can be estimated (Potty et al., 2003). We assume that the ocean acoustic waveguide is stratified and range independent.

First, the times of arrival for the modal amplitude peaks are selected from the dataset to get  $\Delta T_{ii}$  and  $\Delta T_{ji}$ , differences in arrival time along the modes  $i$  and  $j$ .

$$\Delta T_{ii}(f) = \left[ \frac{1}{V_g^i(f)} - \frac{1}{V_g^i(f_H)} \right] r \quad (2.12)$$

In the brackets on the right hand side of Eq. 2.12, the differences between theoretical group speeds of different frequencies within the same mode are compared to a reference frequency. In this equation,  $i$  is the mode of interest for the range

specified  $r$ ,  $f_H$  is a reference frequency different from  $f$ , and  $V_g$  is the theoretical group speed from the inversion, and  $\Delta T_{ii}(f)$  is the observed difference in time of arrival for the different experimental frequencies of a single mode.

The arrival time difference and group velocity difference between two different modes,  $i$  and  $j$  is shown below.

$$\Delta T_{ji}(f) = \left[ \frac{1}{V_g^j(f)} - \frac{1}{V_g^i(f)} \right] r, \quad i \neq j \quad (2.13)$$

The final step is to solve for range by comparing frequencies and times of arrival for different mode pairings. To start, the difference between the left hand side of Eq. 2.12 and Eq. 2.13 compares the travel time difference  $\Delta T(f)$ .

$$\Delta T(f) = \Delta T_{ii}(f) - \Delta T_{ji}(f) \quad (2.14)$$

The difference between the two bracketed right side equations in Eq. 2.12 and Eq. 2.13 is  $K_t(f)$ .

$$K_t(f) = \left[ \frac{1}{V_g^i(f)} - \frac{1}{V_g^i(f_H)} \right] - \left[ \frac{1}{V_g^j(f)} - \frac{1}{V_g^i(f)} \right] \quad (2.15)$$

Combining these two equations, the relationship is linear in the form  $y = mx + b$ , where the slope is range  $r=m$ .

$$\Delta T(f) = [K_t(f)]r \quad (2.16)$$

#### 2.4 Overview of Genetic Algorithm

The genetic algorithm is a method for solving both constrained and unconstrained optimization problems that is based on natural selection, the process

that drives biological evolution. The method consist of three operations: selection, genetic operation, and replacement as highlighted in Figure 5. First, a population is generated randomly within the user specified range for the model parameters. The individuals in the population are evaluated and scored with a fitness value for each generation.

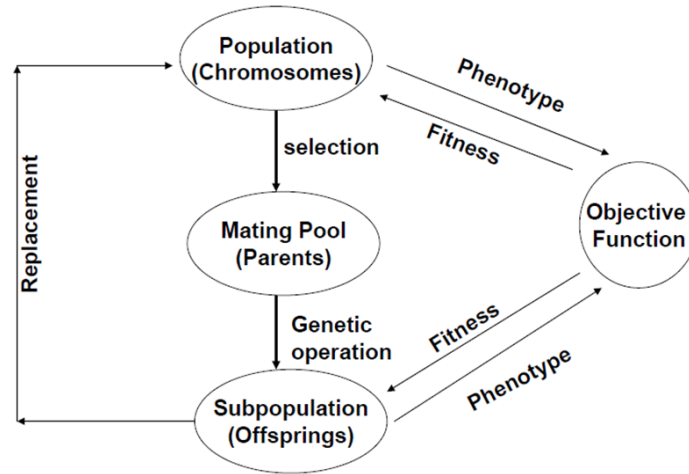


Figure 5. Flow diagram of genetic algorithm optimization (Potty et al., 2000).

Uniform crossover means each parameter of the parent population is randomly swapped into the next generation. Figure 6 below shows the crossover points for a set of parents. Applicable to the experiment, each exchange of the parameters returns a slightly different attenuation value than the previous generation for evaluation. The fittest values are passed on, optimizing the dataset.

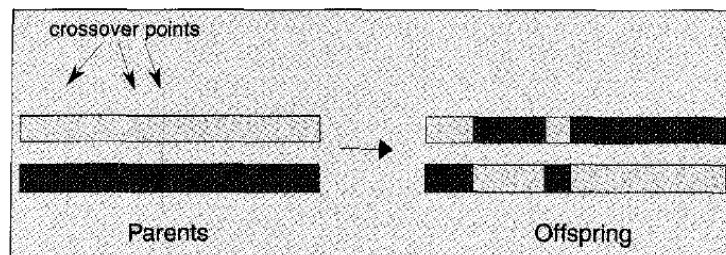


Figure 6. Illustration of crossover between generations during optimization (Tang et al.,1996 ).

In addition to the population exchanges, the offspring can mutate as well. A binary string is generated the same length as the number of parameters being evaluated. A zero indicates there is no exchange, while a one means that parameter evolves for the next generation.

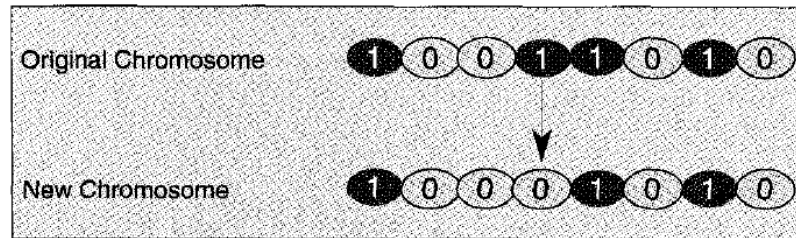


Figure 7. Above, the binary encoding of the parameters for each generation is shown with mutated parameters indicated by a one (Tang et al.,1996 ).

In this analysis, each new population was generated with the same number of individual members to recreate the same population size. To accelerate the algorithm, an elitist strategy was implemented where only the fittest individuals advanced to the next generation.

To maintain diversity in the subpopulations, 20 percent of each population was migrated at random over the course of 20 generations. The migration uses a complete net topology, meaning the individuals were unrestricted in their exchanges between populations as shown in Figure 8.

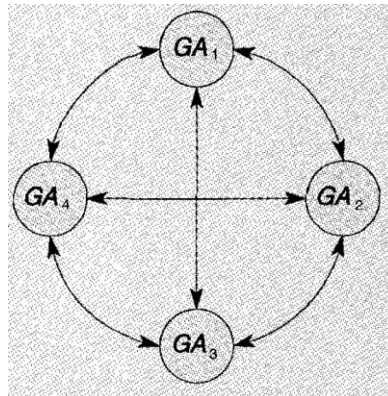


Figure 8. Complete net topology with unrestricted migration during genetic algorithm selection (Tang et al.,1996).

## 2.5 A Posteriori Analysis

During the genetic algorithm optimization, the evolving populations were recorded along with their fitness value for post processing. Based on the procedure outlined in Gerstoft et al. (1994) *a posteriori* statistics can be computed using the model parameter samples. The error analysis procedure is briefly outlined in this section. For a detailed discussion refer to Gerstoft et al. (1994). The probability associated with the model parameters are given by

$$\sigma(m_i) = \frac{e^{-\phi(m_i)/\phi_{50}}}{\sum_{i=1}^{80} e^{-\phi(m_i)/\phi_{50}}}. \quad (2.17)$$

In Eq. 2.17,  $\sigma(m_i)$  is probability,  $i$  is each parameter in a population of  $m_i$  members sorted by fitness. Fitness is equal to  $1 - \phi(m_i)$ .

For our analysis,  $i$  is equal to parameters 1 to 13 that were optimized in this experiment. The *a posteriori* mean is computed using the summation

$$E(m) = \sum_{i=1}^{N_{obs}} m_i \sigma(m_i). \quad (2.18)$$

Covariance is computed using the following equation.

$$\begin{aligned} C(m) &= E\{[m - E(m)][m - E(m)]^T\} \\ &= \sum_{i=1}^{N_{obs}} m_i (m_i)^T \sigma(m_i) - E(m)E(m)^T \end{aligned} \quad (2.19)$$

The square root of the covariance matrix diagonal is used to compute the attenuation coefficient standard deviation for each layer of sediment.

## CHAPTER 3

### EXPERIMENT DESCRIPTION

The Seabed Characterization Experiment (SBCEX) sponsored by the Office of Naval Research (ONR) deployed an assortment of gear just south of Martha's Vineyard in March, 2017. The University of Rhode Island (URI), the Norwegian Defense Research Establishment (FFI), Knobles Scientific and Analysis (KSA), Woods Hole Oceanographic Institution (WHOI), Applied Research Laboratories at the University of Texas at Austin (ARL-UT), Scripps Institution of Oceanography (SIO), the Naval Undersea Warfare Center (NUWC) and others were involved in the experiment. Three oceanographic research vessels were in operation for about three weeks in the Atlantic Ocean: R/V Neal Armstrong, R/V Hugh Sharp, and R/V Endeavor.

#### *3.1 Site Description*

The experiment site was surveyed and cores were collected and analyzed in the prior year (Goff, 2018). Figure 9 shows an overlay of grain size on the site's coastal outline map. Water depth in this area is nominally 70 m. The area under study is known as the New England Mud Patch. This paper concentrates on the SUS data in the northeast corner of the New England Mud Patch in Figure 9.

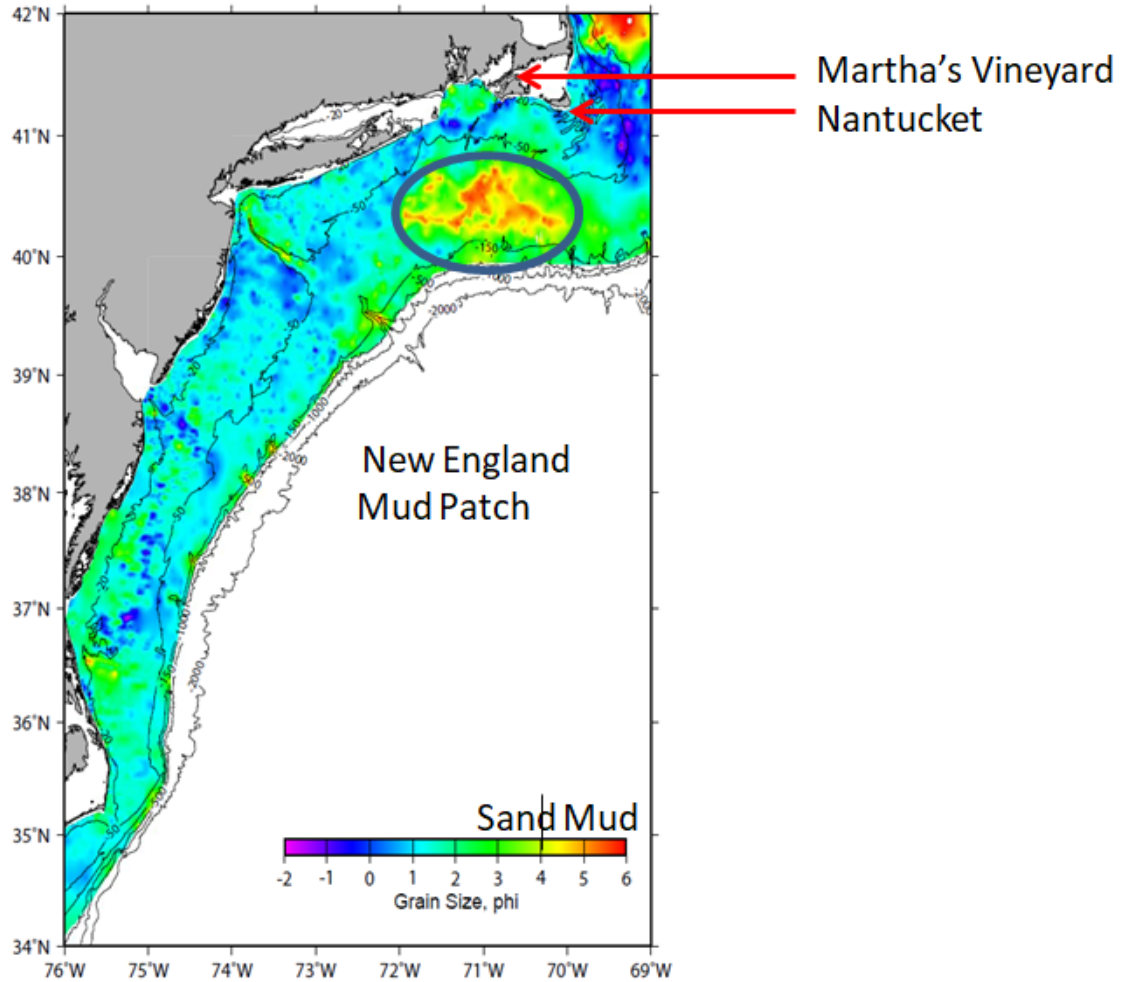


Figure 9. The experiment location is outlined in blue. The color map indicates grain size obtained by survey techniques prior to the experiment (Goff et al., 2018).

### 3.2 Signals, Underwater Sound (SUS) Description

The intent of the experiment was to determine attenuation values from acoustic data collected in conjunction with the detonation of explosives in the water column.

There were two types of explosive sources, the first being Signals, Underwater Sound (SUS). SUS charges were designed as a controlled broadband source (ONR, 1975).

The 31 g MK 64 SUS charges were pressure sensitive to explode at 18 m.

Approximately 200 SUS were deployed at stations in a radial pattern about the array as shown in Figure 10. Five SUS charges were released consecutively at each drop

location about 15 seconds apart. A small subset of SUS charges are the sole focus of this report. The other broadband source in the SBCEX experiment was the Combustive Signal Source (CSS). A CSS is a “high-intensity low-frequency pulse, followed by several weaker bubble pulses” (Bonnel, 2018).

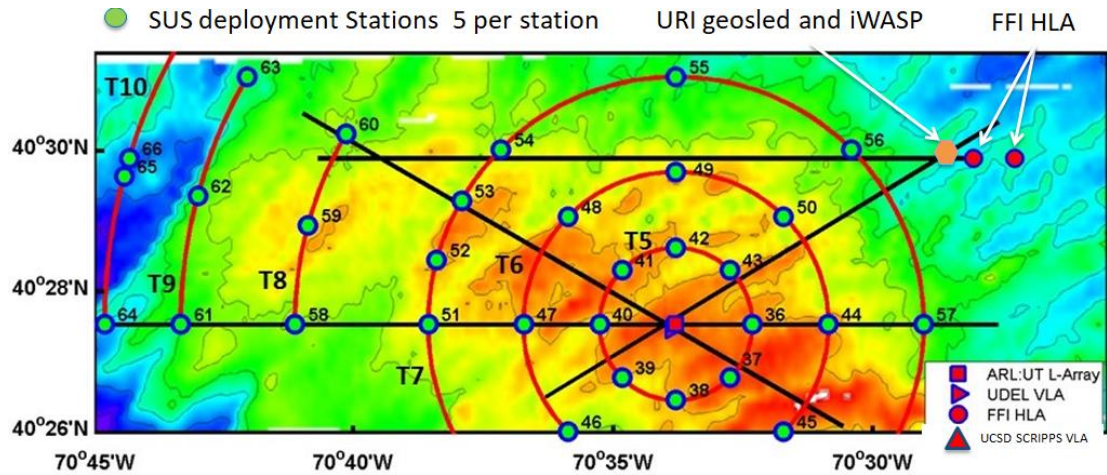


Figure 10. Above is an overhead view of the experimental site. The horizontal line array is positioned to the northeast marked as FFI HLA. The SUS charges deployed are depicted by green circles in a radial pattern (Knobles et al., 2019).

The acoustic receivers in the experiment were a tetrahedral array, geophone array, vertical line arrays, and a two bottom mounted horizontal line arrays. The data processing of the FFI horizontal line array is the basis of this thesis. Data were provided by Dag Tollefsen of the Norwegian Defense Research Institute (FFI).

### 3.3 Horizontal Line Array Description

Data were recorded on a horizontal line array oriented from west to east as shown in the cross section of the experiment set up in Figure 11.

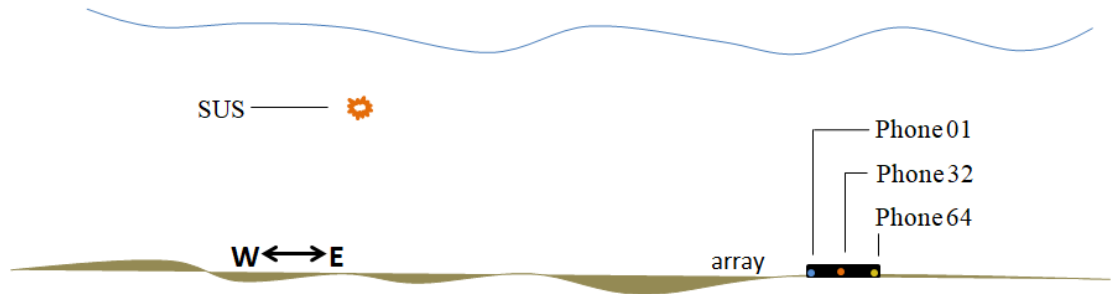


Figure 11. Cross section of the experiment setup.

Locations of the three hydrophones, phone 1, 32 and 64 used in this experiment are shown in Figure 12. There was roughly a kilometer separation between hydrophone 1 and 64.

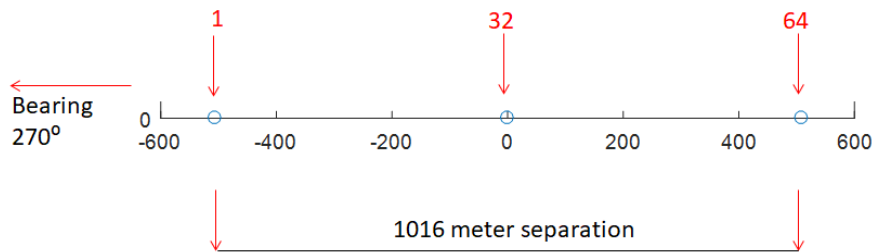


Figure 12. Hydrophones examined on the bottom-mounted horizontal line array.

### 3.4 Environmental Conditions

The nearest maintained National Oceanographic and Atmospheric Administration (NOAA) buoy is serial number 44097 to the southwest of Martha's Vineyard. The buoy recorded data for significant wave height, dominant wave period and direction, average wave period, and sea surface temperature. The significant wave height reduced by approximately 0.3 m between the two deployment times, implying the sea state was gradually decreasing. Wind was fairly constant from the east. The sea surface temperature was a steady 5.8 degrees Celsius (NOAA, 2018).

The spring test date was selected specifically to utilize the nearly isovelocity conditions of the Atlantic Ocean. This minimized the oceanographic effects so the geology was the concentration. The water column sound speed varied 1 m/s over the depth of water as shown in Figure 13. The sound speeds shown below the 70 m interface represent the estimated sediment sound speed values by Julien Bonnel et al. (2018). The 300 m extension of the profile represents the basement layer of the seafloor and was implemented for stability of the model. The lower order modes have longer wavelengths and require a few wavelengths penetration into the sediment to sufficiently model the exponential decay of mode shape  $\psi$ . For instance, the basement sound speed estimate from Figure 14 is roughly 1860 m/s and the lowest frequency examined in this analysis was 20 Hz.

$$\lambda = \frac{c}{f} = \frac{1860 \text{ m/s}}{20 \text{ Hz}} = 93 \text{ m} \quad (3.1)$$

The 300 m depth model of the vertical column should accurately capture three wavelengths of the modes at 20 Hz.

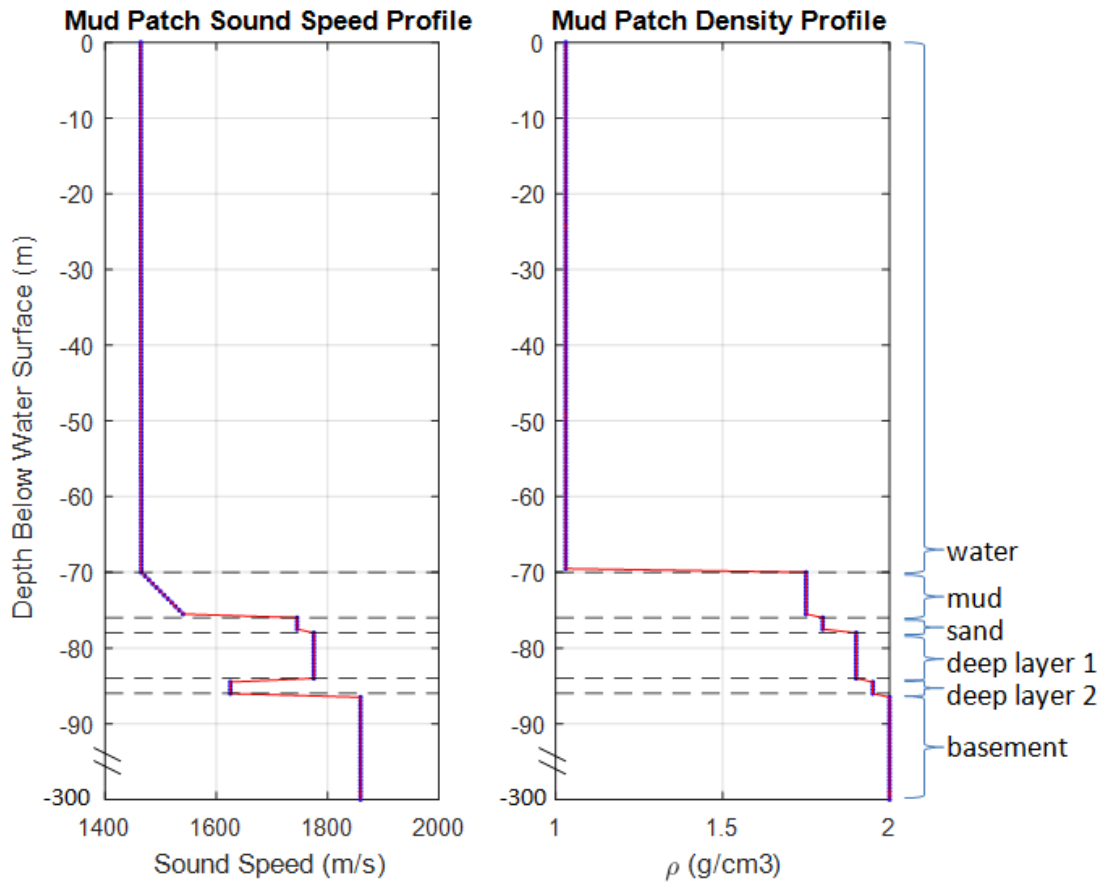


Figure 13. New England Mud Patch sound speed and density profiles obtained by inversion (Bonnel et al., 2018).

The sediment layers shown in Figure 14 were defined by Goff et al. (2018) obtained by survey and coring results collected prior to the experiment. The role of the sound speed and density profiles input into the genetic algorithm for the inversion are described in detail in Chapter 4. A close up of the sediment layers is shown in Figure 14. The mud layer was determined to be 6 m thick.

The characterization of the uppermost layer is the focus of this thesis as its properties heavily influence sound propagation in the ocean.

Water depth: 70m	1464 m/s	1.03 g/cm <sup>3</sup>
	1465 m/s	
Mud: 6 m thick	1540 m/s; 1.75 g/cm <sup>3</sup>	
Sand: 2 m thick	1745 m/s; 1.8 g/cm <sup>3</sup>	
Deep layer 1: 6.5 m thick	1775 m/s; 1.9 g/cm <sup>3</sup>	
Deep layer 2: 1.75 m thick	1625 m/s; 1.95 g/cm <sup>3</sup>	
Basement	1859 m/s; 2.0 g/cm <sup>3</sup>	

Figure 14. The density profile and thickness for the New England Mud Patch sediment boundary layer is shown above. The image is not to scale (Goff et al., 2018).

Deep layer 1, which is 15 m below the water and sediment boundary, is assumed to be sand. Attenuation values in this layer also will be computed. These values are expected to represent sandy sediments and can be used to compare the inversion results to historical data.

## CHAPTER 4

### METHODOLOGY

#### *4.1 Data Selection*

Time frequency signal processing was used to analyze the broadband signal arrival time and amplitude of acoustic normal modes one through four. The frequency band of interest was 20 to 200 Hz. Two SUS deployment locations were used in this thesis from the SBCEX 2017 experiment. The locations were identified as SUS Station 49 and 54 as shown in Figure 15. The deployment location coordinates are shown in Table 2. Both sites were occupied on the same day within a few hours of each other. Station 54 was the westernmost site examined and approximately 13 km away from hydrophone one of the horizontal line array. Station 49 was closer to the array and about 8 km away. A map of all the experimental SUS stations is shown in Figure 15 with the two stations examined in this report boxed in red. Five SUS were dropped at each station. A table of all the SUS station coordinates is available in Appendix A. The first SUS at Station 49 examined in this report, was deployed March 17, 2017 starting at 23:21 UTC. The last SUS at Station 54 completed deployment, 2:15 March 18, 2017.

Table 2. SUS stations listed by deployment date and coordinate.

<b>Time UTC</b>	<b>Latitude</b>	<b>Longitude</b>	<b>Event</b>	<b>Description</b>
3/18/2017 3:21	40.495433	-70.562770	96	SUS 49
3/18/2017 5:51	40.500620	-70.619078	102	SUS 54

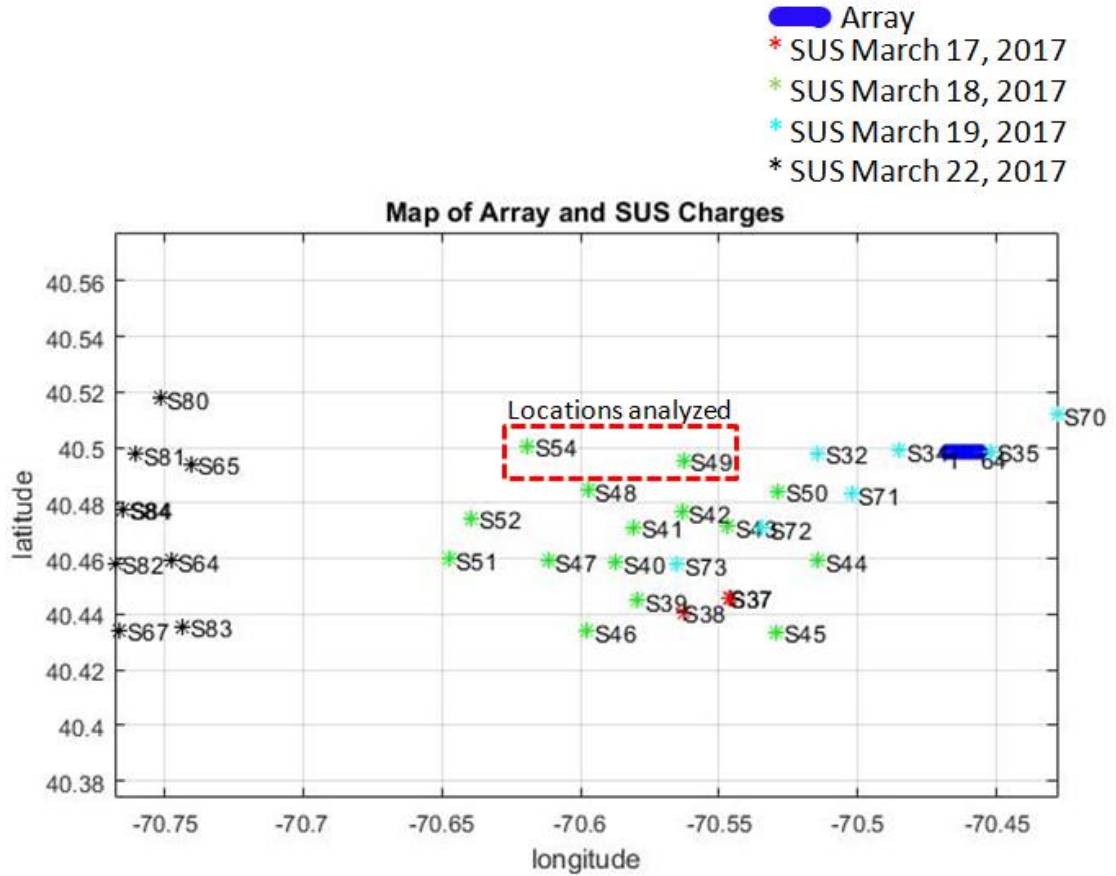


Figure 15. Map of array and SUS charges color-coded to the day of deployment.

Each SUS detonation was extracted with surrounding data. The raw data were plotted for a quality check before being subjected to data analysis. Since there is a kilometer separation between the hydrophones examined, the difference in the pressure wave arrival time varied. Stations 49 and 54 were selected because of their location immediately west of the array for the least range dependent path. The staggering of arrival time is shown in Figure 16. This plot captures a five second span of time across the hydrophones. Hydrophone one at the top was the farthest west and receives the pressure wave first. The data was reviewed for voids during recording and excessive noise before analysis.

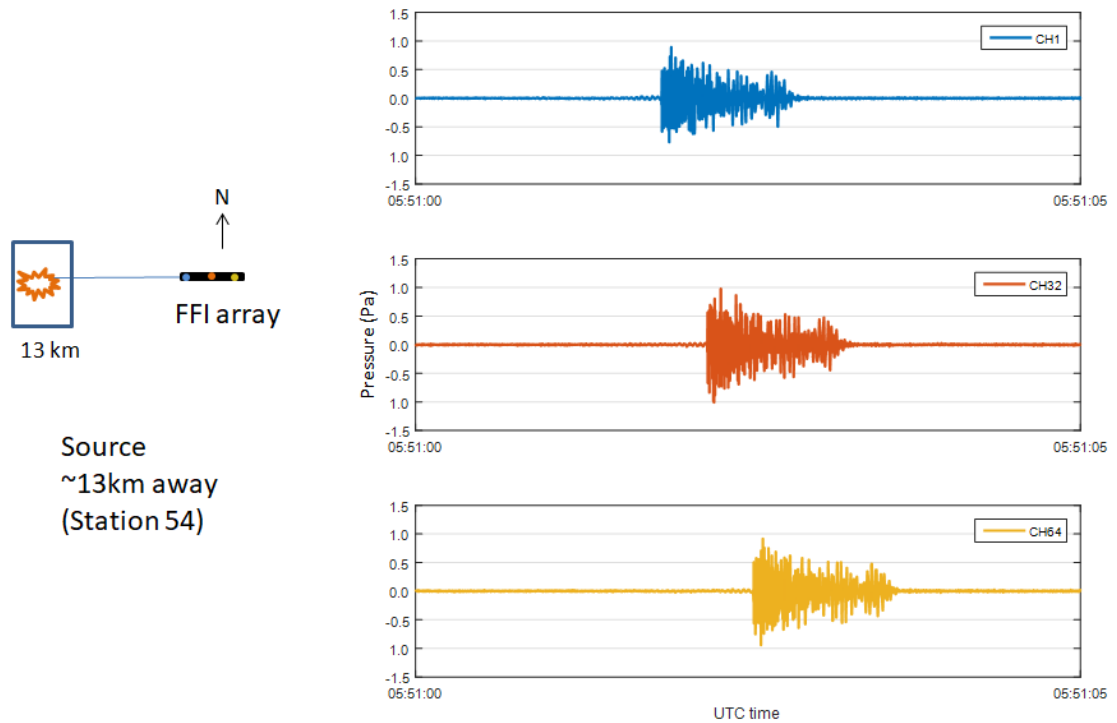


Figure 16. Above, the difference in time of arrival is plotted for the different hydrophones. The hydrophone number is noted to the right.

#### 4.2 Data Processing Overview

Figure 17 captures the data flow explained in detail in the following sections. The techniques and code were developed by Potty et al. (2003). Matrix Laboratory (MATLAB) software and functions were used for data analysis.

First, the experimental data scalograms were examined. The amplitudes of individual normal modes were selected from a frequency slice that focused on bands with significant modal amplitude. This is noted as the ‘observed’ data in the flow diagram. The sound speed, density, and frequencies of interest were assimilated into a matrix for calculating the eigenvalues and eigenfunctions. Next, an acceptable range of theoretical parameters was established, noted as ‘predicted’ in the flow diagram. These variables were used to compute modal attenuation  $\beta_m$  from Eq. 2.11 that was required to create theoretical amplitude ratios for comparison to those measured

## Parameter Optimization Steps

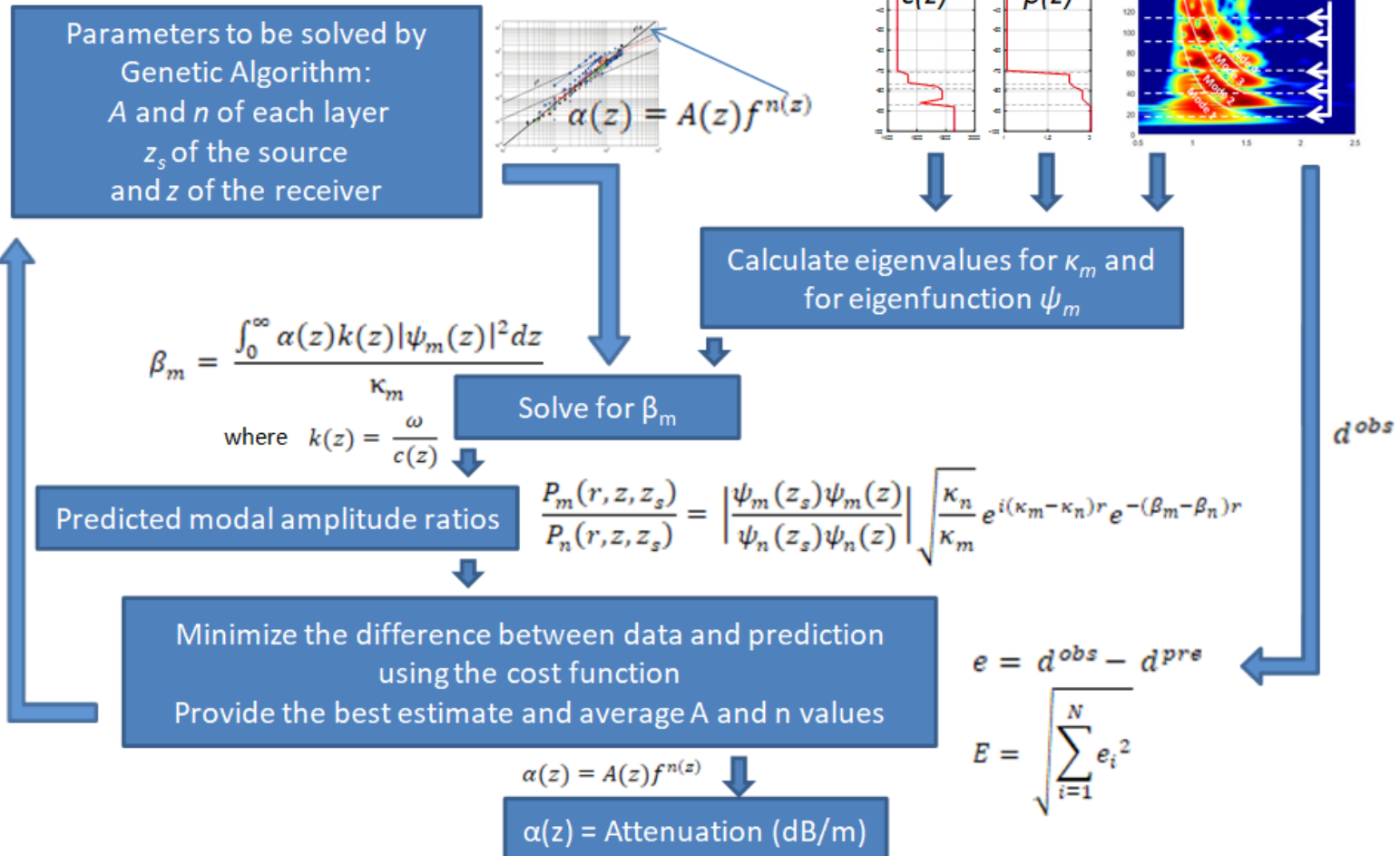


Figure 17. Data flow of parameter optimization using genetic algorithms as developed by Potty et al. in “Inversion for sediment geoacoustic properties at the New England Bight” (2003).

by the experiment. The difference between the experimental and observed ratios were minimized and optimized by genetic algorithms. Finally, the cost function was used to determine the optimal parameters.

#### *4.3 Time-Frequency Analysis for Modal Amplitude Selection*

Data from each SUS charge was imported individually into MATLAB for analysis. First, the data was converted to Pascal by dividing by  $10^6$ . The time series was then normalized by the sampling frequency. A low pass, fourth order Butterworth filter was designed using a cutoff frequency of 500 Hz by the MATLAB function *butter.m*. The data was filtered using the output coefficients. The data was resampled at a rate of 500 Hz.

Next, the analytic signal was derived by taking the Hilbert transform of the real portion of the filtered data signal from the SUS. Morlet wavelet analysis was computed for the signal at increments of 25 samples. Important to note with wavelet transform is reduced high frequency resolution (Wan et al., 2009). The upper and lower frequency bounds were 0.001 to 0.5 in radians. The scalogram is displayed as a color map using the MATLAB *pcolor.m* function. Figure 18 of the scalogram shows intensity as a function of time on the x-axis and frequency on the y-axis, and amplitude was normalized so the peak corresponds to 0 dB.

From the scalogram, the frequency cross-sections of interest were used to extract peak amplitudes in bands of significant modal analysis. The nulls were avoided as shown in Figure 19.

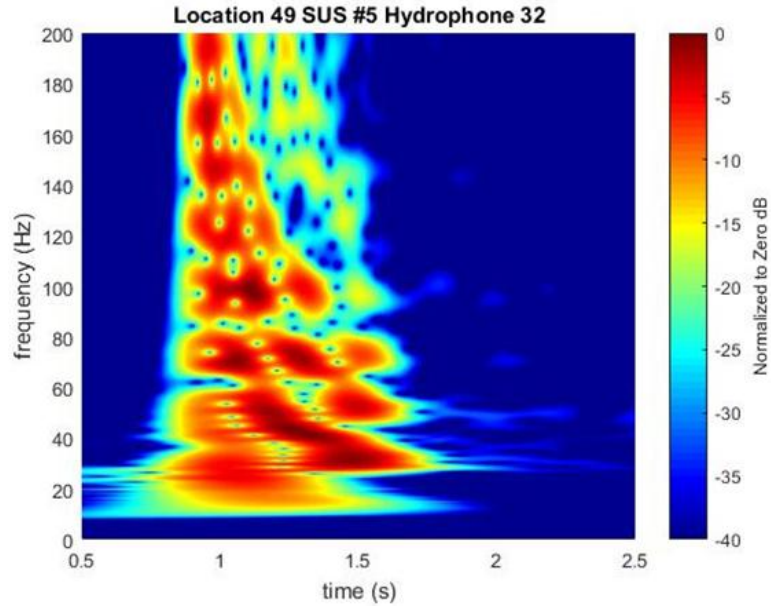


Figure 18. Scalogram of the fifth and last SUS charge deployed at Station 49. The modes are grouped from the lower left corner, starting with mode one through mode four to the upper right in Figure 19. The higher order modes are not as evident and were not considered in this research. There may be some contribution of these higher modes in the lower modes because they were not accounted for.

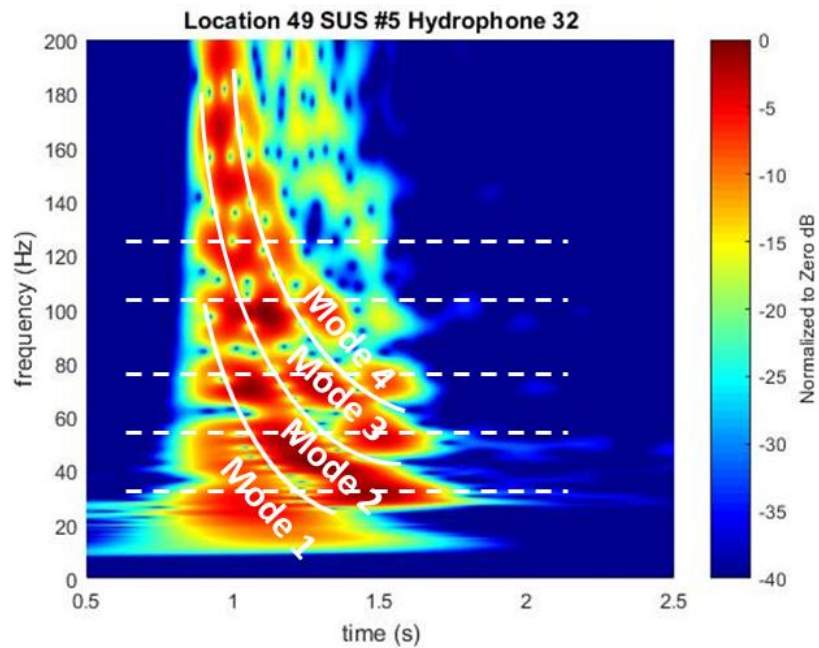


Figure 19. Scalogram of the fifth and last SUS deployed at Station 49, which is the same image as Figure 18. The white dotted lines note the time-frequency slices what were examined for amplitude selection.

The time series slice at each frequency, designated by a white dotted line in Figure 19, was evaluated for modal amplitude selection shown in the upper portion of Figure 20. The maximum amplitude for each mode was selected and recorded. The amplitude is the y-value in the time series in Figure 20 and noted in Table 3. These amplitude values were compared as a ratio for each hydrophone and used to evaluate attenuation.

The MATLAB function *oct3dsgn.m* was used to evaluate the filter coefficients based on the center frequency specified by frequency amplitude correlation on the scalogram. The decimated sampling rate and an order of three were input parameters.

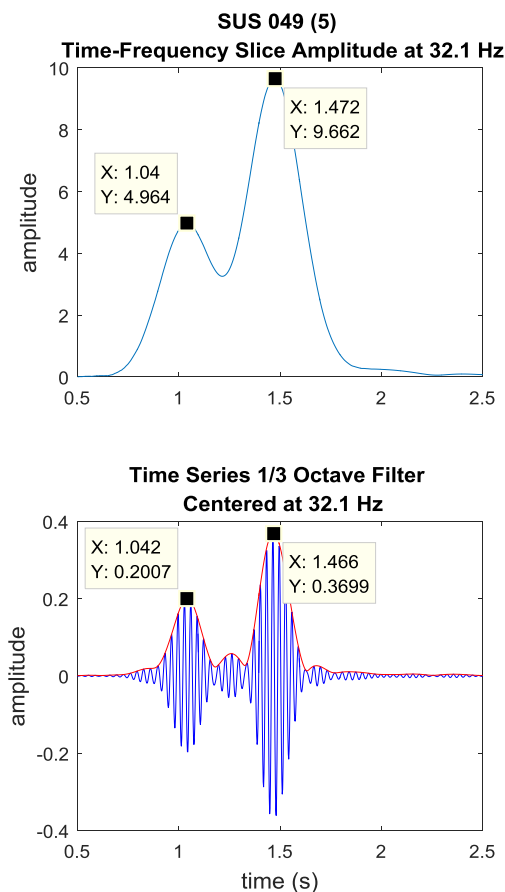


Figure 20. Time series at the frequency slice 32.1 Hz from the fifth and last SUS at Station 49 is shown. The upper image depicts the time-frequency slice, while the lower image utilized a third octave filter demodulate of the same signal.

The filter output is demodulated using the MATLAB quadrature amplitude demodulation *demod.m* command (MATLAB 2018). The magnitude of the complex signal is drawn in red for the lower portion of Figure 20.

Table 3. The table lists amplitude in decibels of modes one through four, calculated for each hydrophone during the fifth SUS detonation at Station 49.

		frequency (Hz)					
		Sensor	32.1	53.1	72.4	99.3	122.1
Modes 1-4	M1	1	0.1721	0.1405			
	M2	1	0.3486	0.3484	0.3887	0.3419	
	M3	1		0.2754	0.36	0.4796	0.2698
	M4	1			0.1946	0.2836	0.1885
	M1	32	0.2007	0.1616	0.1945		
	M2	32	0.3699	0.3684	0.4348	0.3837	0.2878
	M3	32		0.3107	0.3713	0.476	0.3612
	M4	32			0.1931	0.257	0.2264
	M1	64	0.1816	0.1517	0.1686		
	M2	64	0.3443	0.3771	0.4346	0.3837	0.3408
	M3	64		0.2967	0.392	0.476	0.3596
	M4	64			0.1681	0.257	0.2037

Occasionally, the amplitude at hydrophone 64 is higher than the amplitude at hydrophone one although it is farther away from the source. For example, mode two for hydrophone 64 was recorded at 0.3771 at the frequency 53.1 Hz, while mode two for hydrophone 1 and 32 are lower in amplitude in Table 3. A calibration value was not applied to each hydrophone, resulting in arbitrary amplitude values. However, because the analysis computes ratios at each hydrophone individually, this discrepancy was inconsequential.

### 4.3 Calculation of Experimental Modal Amplitude Ratios

The modal amplitudes entered into Table 3 were copied into the *calcAmpRatio.m* script listed in Appendix B to compute the amplitude ratios. These experimental values were compared to the predicted data generated by the genetic algorithm optimization. The amplitude ratios were computed at a single hydrophone, which made the computations range independent. The modal amplitude ratios used in the computations for each SUS were the following:

- The ratio of Mode 1 and Mode 2.
- The ratio of Mode 2 and Mode 3.
- The ratio of Mode 1 and Mode 3.
- The ratio of Mode 2 and Mode 4.
- The ratio of Mode 3 and Mode 4.

The mode ratio sets are  $d^{obs}$  in Figure 17.

### 4.4 Parameter Descriptions for Genetic Algorithm Computation

The *atten\_opt.m* function in Appendix B, establishes the parameters for the genetic algorithm computations. Genetic algorithm optimization was performed using the standard settings of the Matrix Laboratory Genetic and Evolutionary Algorithm (MATLAB GEA) Toolbox compiled by Hartmut Pohlheim (2006). A description of genetic algorithms is available in Chapter 2.

The inputs into the genetic algorithm were the upper and lower bounds of the parameters under evaluation in Table 4. For the first population generation, a matrix of random variables from zero to one was multiplied by a uniform distribution between the upper and lower bounds of each variable. This created a randomized starting

population generation that was evaluated for fitness, where only the best individuals were passed to the next generation. The mutation probability setting was  $\frac{1}{13}$  for the 13 parameters being evaluated.

In this thesis, the  $A$  and  $n$  parameters were optimized to compute the attenuation profile as a function of depth  $\alpha(z)$  for each sediment layer. The effective attenuation coefficient is represented by the relation

$$\alpha(z) = A(z)f^{n(z)} \quad (4.1)$$

where  $A$  and  $n$  are depth dependent constants,  $f$  is frequency in kHz, computed for each frequency utilized during experimental data amplitude ratio selection, and  $\alpha(z)$  is in nepers per meter. To convert  $\alpha$  from nepers per meter to decibels per meter, the following equation is used

$$\alpha \left( \frac{dB}{m} \right) \equiv -20 \log \frac{A}{A_0} \simeq 8.686 \alpha x \Rightarrow 8.686 \alpha \quad (4.2)$$

where  $A_0$  is the root mean square amplitude at  $x = 0$  (Jensen, 1994).

Table 4. Thirteen parameters were optimized by the genetic algorithm.

Variable	Parameter	Lower Bound	Upper Bound	Unit
1	A of layer 1 (mud)	0.0025	0.0900	n/a
2	n of layer 1 (mud)	1.0	2.0	n/a
3	A of layer 2 (sand)	0.0025	0.0900	n/a
4	n of layer 2 (sand)	1.0	2.0	n/a
5	A of layer 3 (deep layer 1)	0.0025	0.0900	n/a
6	n of layer 3 (deep layer 1)	1.0	2.0	n/a
7	Depth of source 18+Bounds	-1.0	1.0	m
8	Receiver depth increment 69.5+Bounds	-1.5	1.5	m
9	A of layer 4 (deep layer 2)	0.0025	0.0900	n/a
10	n of layer 4 (deep layer 2)	1.0	2.0	n/a
11	A of layer 5 (basement)	0.0025	0.0900	n/a
12	n of layer 5 (basement)	1.0	2.0	n/a
13	$\alpha$ of layer 5 (basement)	0.0001	0.0004	dB/m

The attenuation value in Eq. 4.1 was utilized in the MATLAB code *atten\_main\_5layer.m*, which calls the *beta\_5layer.m* available in Appendix B. These two scripts focus on solving modal attenuation  $\beta_m$  from Eq. 2.11.

#### 4.5 Calculation of Theoretical Modal Amplitude Ratios

Recall the compressional wave pressure Eq. 2.8 from Chapter 2 for a single hydrophone. This equation sums the normal modes  $M$  to represent the far field acoustic pressure, where  $r$  is range,  $z$  is the depth at the receiver,  $z_s$  is the depth of the source,  $\rho$  is the density at the source,  $\psi_m$  is the  $m$ th mode shape,  $\kappa_{rm}$  is the horizontal wave propagation constant, and  $\beta_m$  is the modal attenuation coefficient from Eq. 2.11. The modal attenuation coefficient relies on the optimized parameters from the genetic algorithm in Section 4.4 for computation of effective attenuation  $\alpha$ . A theoretical amplitude pressure needs to be computed for each mode compared in the amplitude ratios of Section 4.3. The theoretical modal amplitude ratio is the following.

$$d^{pre} = \frac{P_m(r, z, z_s)}{P_n(r, z, z_s)} = \left| \frac{\psi_m(z_s)\psi_m(z)}{\psi_n(z_s)\psi_n(z)} \right| \sqrt{\frac{\kappa_n}{\kappa_m}} e^{i(\kappa_m - \kappa_n)r} e^{-(\beta_m - \beta_n)r} \quad (4.3)$$

In Eq. 4.3,  $m$  and  $n$  are two different normal modes at the same hydrophone,  $\rho$  is medium density,  $r$  is the source to receiver range,  $z$  is the receiver depth,  $z_s$  is the source depth,  $\psi$  is the mode shape for the mode under examination for modes  $m$  and  $n$ ,  $\kappa$  is the horizontal propagation constant of each mode, and  $\beta$  is the intrinsic modal attenuation coefficient obtained by inverse methods. The *amp\_ratio.m* script in the Appendix B computes the predicted modal amplitude ratio.

The computation of the variables required to obtain the theoretical amplitude ratio are described in the remainder of this section.

The mode shapes  $\psi_m$  are computed first and substituted into the  $\beta_m$  from Eq. 2.11. Code called *zmode.m* from the Ocean Acoustic Library archive was used (Ocean Acoustic Library). The Ocean Acoustic Library script solves for the following system equation.

$$[A - \kappa_m^2 I]\psi_m = 0 \quad (4.4)$$

$I$  is the identity matrix of length  $N$  for the number of  $\kappa_m$  eigenvalues, and  $\psi_m$  are the eigenvectors obtained. The  $A$  matrix is an assimilation of the frequencies selected from the observed amplitude ratios and sound speed  $c$  for each increment of depth  $z$ . The resulting matrix of  $\psi_m$  eigenvectors is sorted by ascending columns. The square root of each the first four eigenvalues is the  $\kappa_m$  value horizontal propagation constant term for each mode (Ocean Acoustics Library). The eigenfunctions are then normalized and passed to Eq. 2.11 and Eq. 4.3.

Lastly, the range  $r$  between the array hydrophone and the SUS charge is computed using the script *sw\_dist.m* (Morgan ,1992). The first input to the function is the SUS latitude as provided by the waypoints in Appendix A and the hydrophone latitude. The second inputs are the respective longitudes. The output is separation in kilometers.

#### 4.6 Error Minimization

The predicted amplitude ratios are then compared to the observed amplitude ratios for each frequency. The difference between predicted and observed is the error and is given by

$$e = d^{obs} - d^{pre} \quad (4.5)$$

In this equation,  $e$  is the error vector,  $d^{obs}$  is the observed amplitude vector by frequency, and  $d^{pre}$  is the predicted amplitude vector by inversion matched to the observed frequencies.

The error  $e$  for each ratio from the different SUS was assimilated into an overall error to evaluate the current population computed by the genetic algorithm. The cost function, also known as the objective function, was used to quantify the fitness of the parameters under evaluation by minimizing the cumulative sum of the square of the residuals.

Each station was combined into a joint optimization problem. Both experiment Station 49 and Station 54 were evaluated as a whole using the cost function, summing the squares of the five SUS charges and the resulting five sets of amplitude ratios at a single hydrophone. The best and average of the sets of individual parameters are compared in *a posteriori* analysis and to historical data in Section 5.3.

## CHAPTER 5

### RESULTS

The goal of this research is to establish a depth dependent attenuation coefficient of the mud layer in the New England Mud Patch. Equation 4.1 is evaluated using the estimated  $A$  and  $n$  parameters output by the genetic algorithm as a function of depth.

#### *5.1 A Posteriori Analysis of Depth Dependent Attenuation*

Throughout the genetic algorithm optimization, the population of the evolving generations was saved. These were then used to calculate the *a posteriori* mean and standard deviations of the model parameters as outlined in Section 2.5. Table 5 summarizes the individual parameter results and computed standard deviations.

Table 5. Summary of *a posteriori* statistical analysis for each parameter on all SUS for Stations 49 and 54.

<b>Parameter</b>	<b>Description</b>	<b>Mean Value and Standard Deviation</b>	<b>Unit</b>
1	A of layer 1 (mud)	$0.0054 \pm 0.01$	n/a
2	n of layer 1 (mud)	$1.9 \pm 0.14$	n/a
3	A of layer 2 (sand)	$0.0283 \pm 0.01$	n/a
4	n of layer 2 (sand)	$1.4 \pm 0.22$	n/a
5	A of layer 3 (deep layer 1)	$0.0190 \pm 0.01$	n/a
6	n of layer 3 (deep layer 1)	$1.4 \pm 0.16$	n/a
7	Depth of source	$17.1 \pm 0.2$	m
8 (hydrophone 1)	Receiver depth increment	$70.7 \pm 0.6$	m
8 (hydrophone 32)	Receiver depth increment	$70.5 \pm 0.5$	m
8 (hydrophone 64)	Receiver depth increment	$70.7 \pm 0.5$	m
9	A of layer 4 (deep layer 2)	$0.0309 \pm 0.02$	n/a
10	n of layer 4 (deep layer 2)	$1.5 \pm 0.18$	n/a

11	A of layer 5 (basement)	$0.0357 \pm 0.02$	n/a
12	n of layer 5 (basement)	$1.6 \pm 0.17$	n/a
13	$\alpha$ of layer 5 (basement)	$0.0002 \pm 0.0001$	dB/m

The results of depth dependent attenuation are plotted for 50 Hz as shown in Figure 21 and Figure 22. Figure 21 displays the best genetic algorithm estimate in that they have the lowest misfit for the three locations on the array. Each line on the plot is an independent hydrophone inversion. The average results in Figure 22 correspond to the *a posteriori* mean estimate and are consistent with the best estimate, merely dampened. Since each hydrophone trace follows a similar shape among the group, there is confidence in the results. The standard deviation is roughly ten percent of the attenuation coefficient, indicating a good estimate as well.

Figure 23 and Figure 24 demonstrate the frequency dependence of the sediment profile. The effective attenuation coefficients at the frequencies 30, 75, and 120 Hz are compared on the same axis. The standard deviation is included to the right. Figure 23 displays the best genetic algorithm outputs and Figure 24 is the *a posteriori* mean computed as discussed in Section 2.5. The depth attenuation coefficient profiles are available in Appendix C for Station 49.

Within each of the depth dependent attenuation figures, the first 6 m are expanded in the inner box in red, representing the mud layer. The mud has low attenuation that could not be read on the larger range.

Best Attenuation Coefficients for Station 54 Phones 1, 32, and 64 SUS #1-5

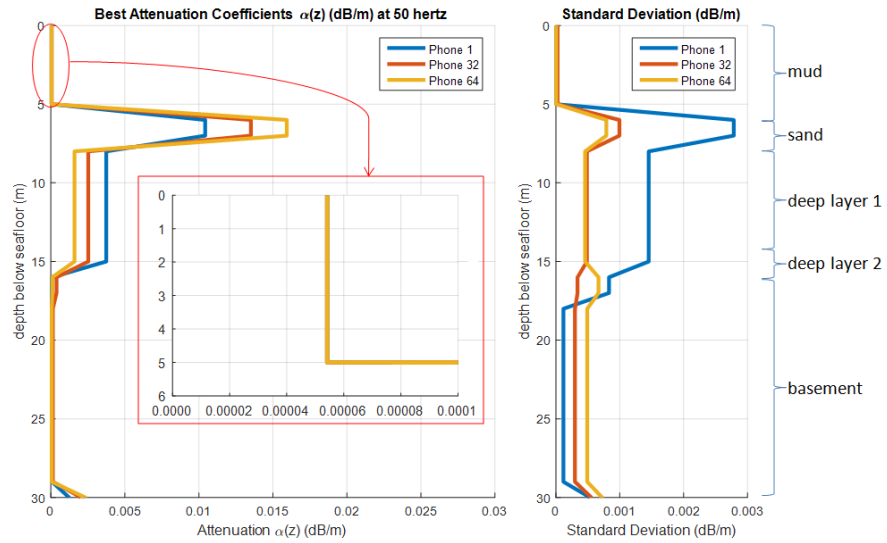


Figure 21. Above are the genetic algorithm lowest misfit parameters and standard deviation for each layer. The mud layer is expanded in the red box.

*Posteriori* Mean Attenuation Coefficients for Station 54 Phones 1, 32, and 64 SUS #1-5

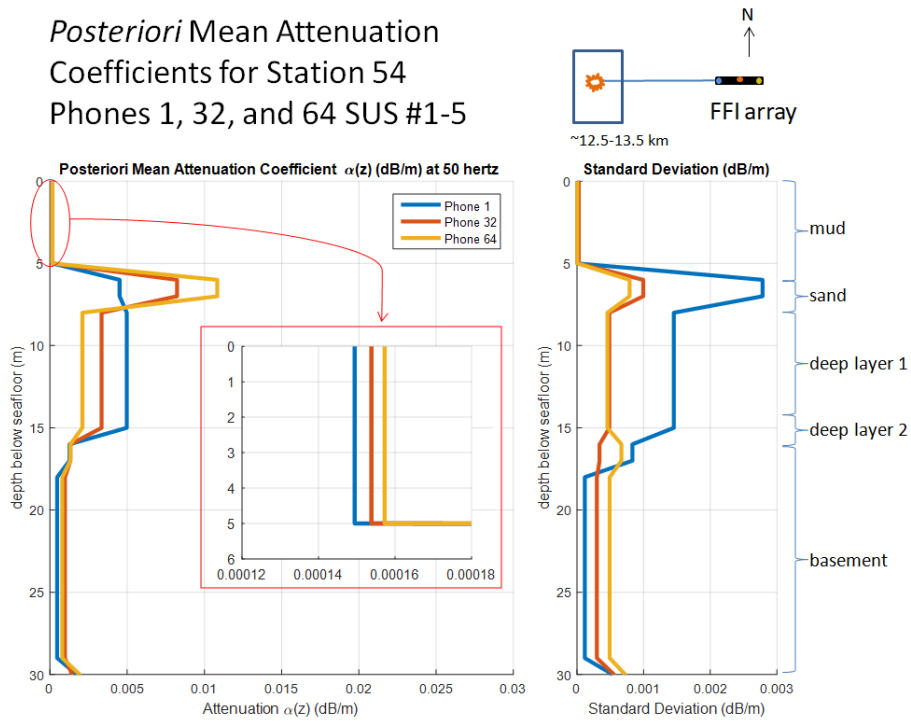


Figure 22. Above is the *a posteriori* average of the 50 lowest misfit parameters for each layer and standard deviation. The mud layer is expanded in the red box.

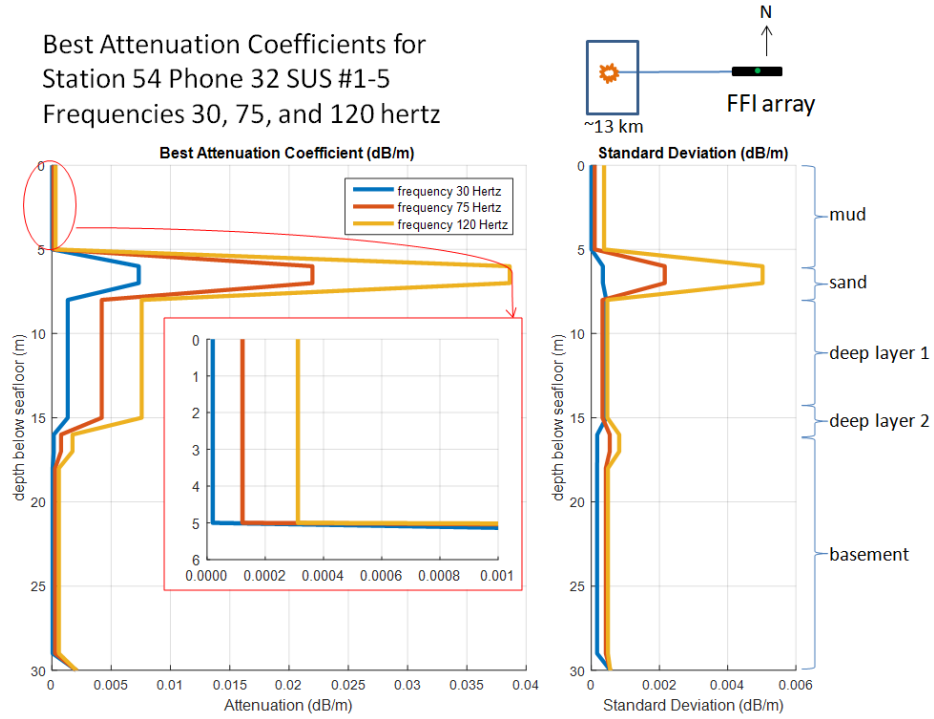


Figure 23. Above are the genetic algorithm best output parameters demonstrating attenuation dependence on frequency. The mud layer is expanded in the red box.

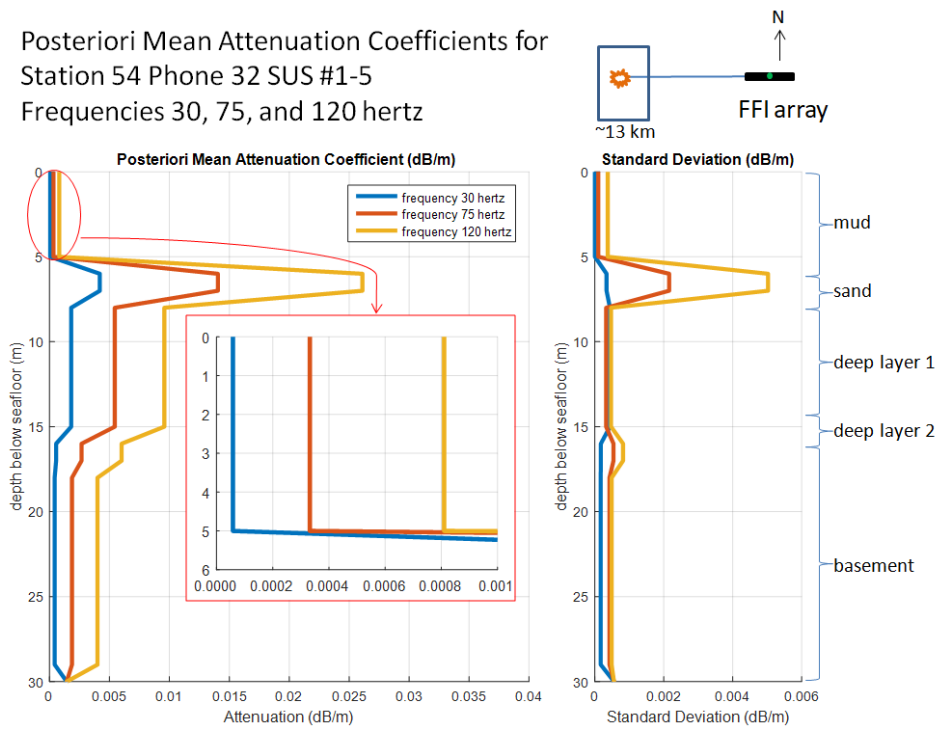


Figure 24. Above are the *a posteriori* average output parameters demonstrating attenuation dependence on frequency. The mud layer is expanded in the red box.

## 5.2 Range Verification

Range verification using group velocity was used to independently verify the assumption of range independence and bottom model. This technique is described in Section 2.3.

First, the times of arrival for the modal amplitude peaks are selected as shown in the scalogram (left panels of Figure 25 and Figure 26) for the first SUS at Station 49 and 54, respectively. The selections are shown as a white asterisk for input into Eq.2.14. Similar to the frequency slice technique in Chapter 4.3 where nulls were avoided, the modes were noted for time of arrival and frequency at the peak amplitudes in two vectors.

The plot of Eq. 2.15 versus Eq. 2.14, results in the right panels of Figure 25 and Figure 26, where the range  $r$  is the slope of the best fit line.

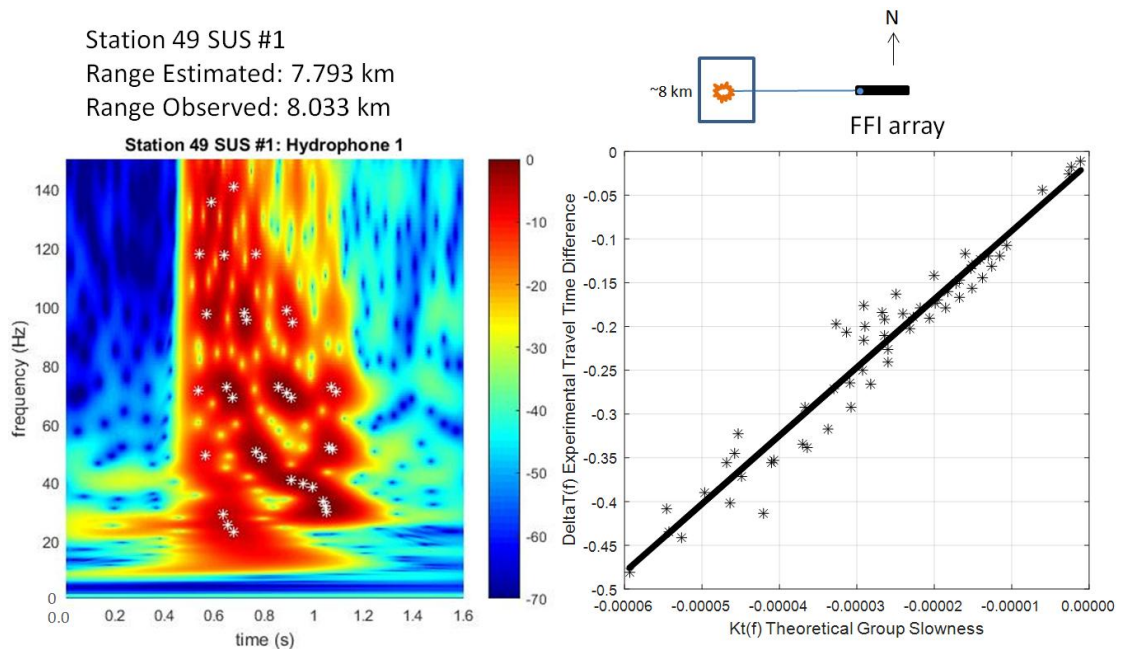


Figure 25. To the left, time of arrival and frequency are selected by peak modal amplitude from the experimental data. To the right, theoretical group velocity difference by mode on the x-axis is compared to experimental travel time difference

on the y-axis. Data is from the first SUS charge deployed at Station 49 approximately 8 km away from hydrophone one on the array.

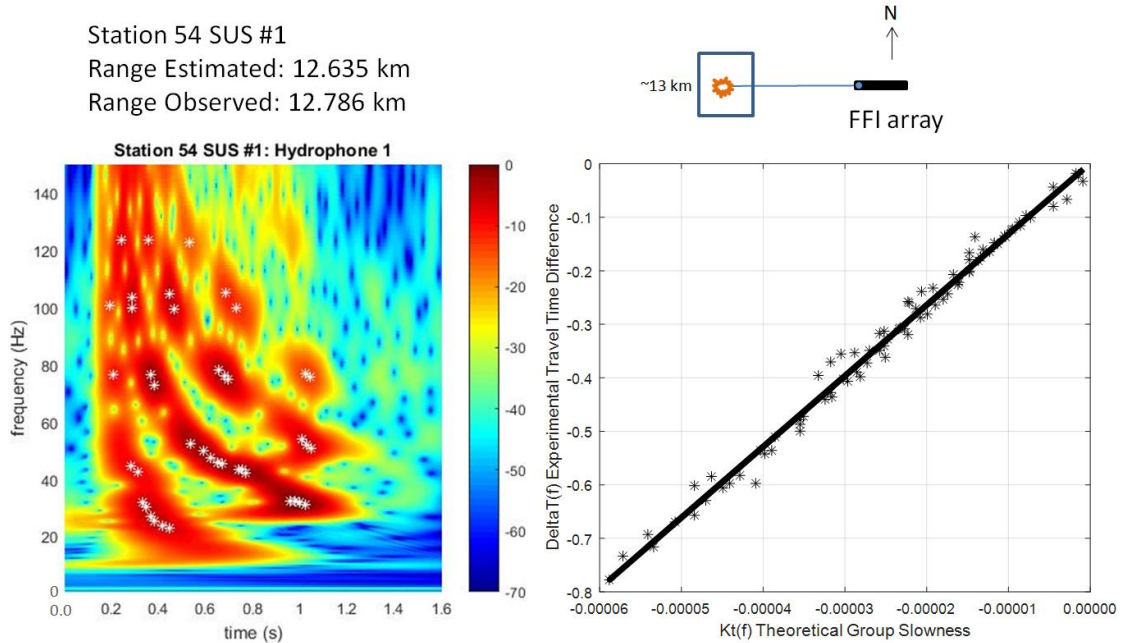


Figure 26. To the left, time of arrival and frequency are selected by peak modal amplitude from the experimental data. To the right, theoretical group velocity difference by mode on the x-axis is compared to experimental travel time difference on the y-axis. Data is for the first SUS charge deployed at Station 54 approximately 13 km away from hydrophone one on the array.

The source to receiver ranges for Station 49 and 54 were independently verified within 150 to 200 m giving confidence to the inversion compressional wave speed. The estimated (from the GPS locations of the source and receiver) range and the calculated range (using the present technique) are shown in Figure 25 and Figure 26. A discrepancy of 150 to 200 m is of the magnitude of 1 to 2 wavelengths at the low frequency range and is not significant, but may indicate some slight range dependence. Any uncertainty in the GPS positions of the source and deployed location of the receiver will also be reflected in the discrepancy.

### 5.3 Comparison to Historic Data

We computed effective attenuation coefficients  $\alpha(z)$  for a frequency range of 30 to 120 Hz and overlaid the results on Figure 27. Figure 27 is a compilation of attenuation values of sand published by Zhou et al. (2009). Attenuation coefficient estimates corresponding to deep layer 1 are shown in yellow triangles and these values match the published data well. Deep layer 1 is assumed to be sand based on core data (Goff et al., 2018). Although the deep layer 1 slope is slightly different from the historical data, it is consistent with the previous inversions from the nearby Primer experimental location, shown in black triangles (Potty et al., 2003). The frequency exponent of the attenuation equation for deep layer 1 (sand) was 1.4 in Table 5. The attenuation coefficient for sand was approximately  $10^{-3}$  (dB/m), varying slightly with frequency.

The mud layer attenuation, shown in brown triangles, is an order of magnitude lower than sand. The frequency exponent of the attenuation equation for mud averaged about 1.9 as shown in Table 5. The mud attenuation coefficient values range from  $10^{-5}$  to  $10^{-4}$  (dB/m) depending on the frequency.

Included on Figure 27 are a few reference points for seawater at 0.5, 1, and 2 kHz depicted as blue triangles. The mud layer split the difference between the sand and water, but is slightly closer to sand. The average attenuation coefficient is computed for the entire 6 m layer of mud, meaning some of the more dense sediment at the bottom of the layer is averaged with the more fluid upper mud layer.

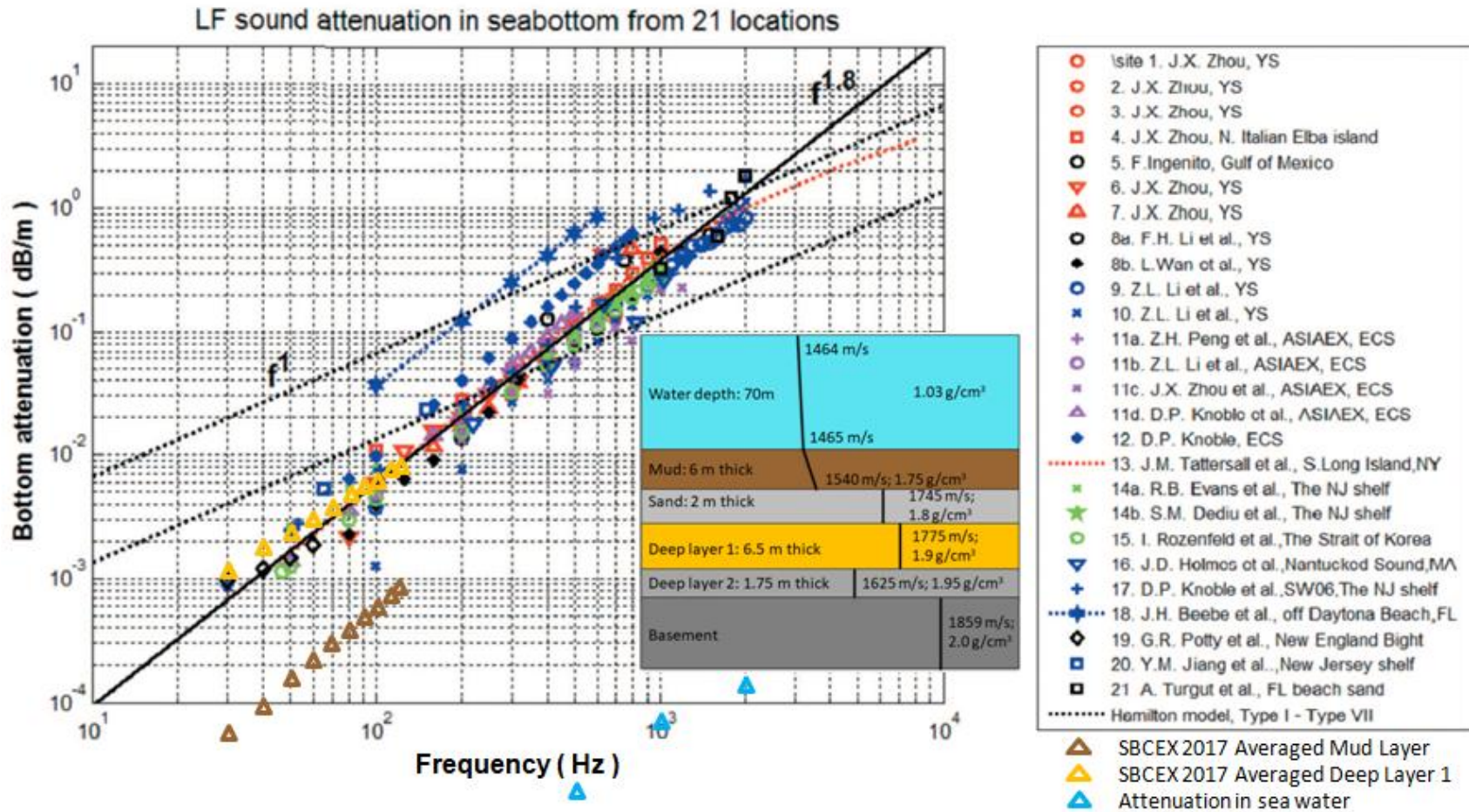


Figure 27. SBCEX average attenuation coefficient  $\alpha(z)$  for Station 49 and 54 overlaid published experimental results. The seafloor surface mud layer is shown in cyan and the deep layer one is in magenta (Zhou et al., 2009).

#### 5.4 Sensitivity Analysis

A sensitivity study of attenuation with respect to depth was conducted *a posteriori*. Figure 28 shows the effect of a ten percent perturbation in  $\alpha(z)$  at various depths on the cost function that was then normalized.

$$\Delta E = E' - E \quad (5.1)$$

$$\Delta E / \|E\| \quad (5.2)$$

In Eq. 5.1,  $E$  is the original cost function corresponding to the un-perturbed model parameters,  $E'$  is the result with a modified (perturbed by 10%) set of model parameters and  $\Delta E$  is the difference. The resulting sensitivity is the normalized  $\Delta E$  plotted in Figure 28.

The interpretation of this plot indicates the deeper layer was as sensitive to changes in effective attenuation  $\alpha$  as the topmost mud layer.

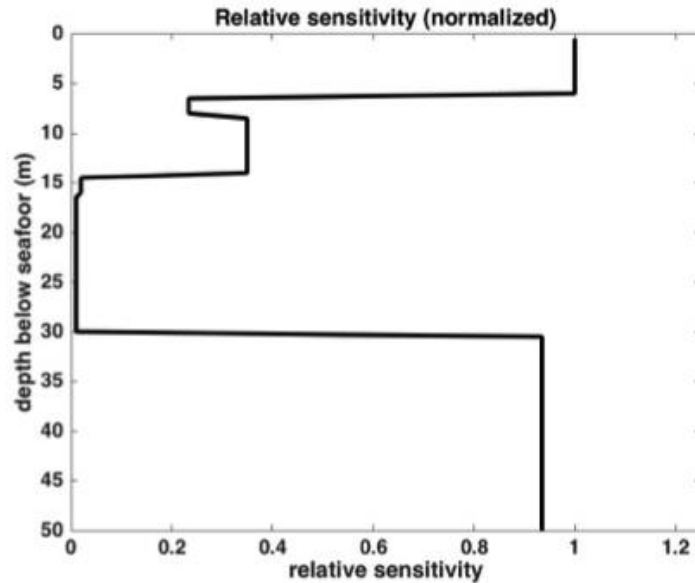


Figure 28. This plot examines the sensitivity of attenuation as a function of depth. A 10% perturbation of attenuation was applied at various depths (Potty et al., 2018).

## CHAPTER 6

### CONCLUSION

To summarize, we studied acoustic pressure from a SUS charge at various ranges on a bottom-mounted horizontal line array. We implemented an inversion scheme for depth dependent attenuation using modal amplitude ratios. The amplitude ratios were taken at a single hydrophone, eliminating need to know the exact source level of the SUS charges. Deep layer 1 of the New England Mud Patch experiment area, presumed to be sand, has attenuation frequency dependence in agreement with published data for sandy sediments as shown in Figure 27. Attenuation in the mud layer was low compared to the sandy sediments. The frequency exponent of mud was 1.9 and the mud attenuation values range from  $10^{-5}$  to  $10^{-4}$  (dB/m), depending on frequency, with a standard deviation of roughly ten percent. The attenuation of water is an order of magnitude lower than mud, placing the attenuation coefficient of mud between the sand and water as hypothesized. Additionally, the source-receiver range was estimated assuming range-independence and the estimates were in close agreement with GPS derived range values. It should be noted that the attenuation estimates were carried out assuming range independence and shear effect was not considered in this study. Shear conversion effects may be an important factor in computing the deep layer attenuation coefficient (Potty, 2018).

## APPENDICES

### *Appendix A. Field Log Excerpt for SUS Charge Recordings*

<b>Time UTC</b>	<b>Latitude</b>	<b>Longitude</b>	<b>Event</b>	<b>Description</b>
3/17/2017 23:17	40.445966	-70.546065	86	SUS S37
3/17/2017 23:32	40.440804	-70.562705	87	SUS S38
3/18/2017 0:03	40.444868	-70.579458	88	SUS S39
3/18/2017 0:20	40.458492	-70.587269	89	SUS S40
3/18/2017 0:38	40.471256	-70.580579	90	SUS S41
3/18/2017 0:55	40.476795	-70.563554	91	SUS S42
3/18/2017 1:13	40.471778	-70.546877	92	SUS S43
3/18/2017 1:34	40.459189	-70.514151	93	SUS S44
3/18/2017 2:14	40.433474	-70.529265	94	SUS S45
3/18/2017 3:00	40.484292	-70.528541	95	SUS S50
3/18/2017 3:21	40.495433	-70.56277	96	SUS S49
3/18/2017 3:42	40.484616	-70.597358	97	SUS S48
3/18/2017 4:05	40.45934	-70.61177	98	SUS S47
3/18/2017 4:31	40.43402	-70.597579	99	SUS S46
3/18/2017 5:07	40.459786	-70.647371	100	SUS S51
3/18/2017 5:27	40.474409	-70.639363	101	SUS S52
3/18/2017 5:51	40.50062	-70.619078	102	SUS S54
3/19/2017 1:32	40.457914	-70.564947	145	SUS S73
3/19/2017 2:02	40.470887	-70.534374	146	SUS S72
3/19/2017 2:23	40.483216	-70.502313	147	SUS S71
3/19/2017 2:48	40.498737	-70.452009	148	SUS S35
3/19/2017 3:06	40.51194	-70.42824	149	SUS S70
3/19/2017 3:38	40.498872	-70.484969	150	SUS S34
3/19/2017 4:01	40.497916	-70.514283	151	SUS S32
3/22/2017 13:09	40.459209	-70.747498	164	SUS S64
3/22/2017 13:41	40.494052	-70.740575	165	SUS S65
3/22/2017 14:26	40.517919	-70.751535	166	SUS S80
3/22/2017 14:45	40.497726	-70.760269	167	SUS S81
3/22/2017 15:17	40.458152	-70.767976	168	SUS S82
3/22/2017 15:37	40.434204	-70.766262	169	SUS S67
3/22/2017 15:55	40.435524	-70.743405	170	SUS S83
3/22/2017 16:47	40.477916	-70.765028	171	SUS S84
3/22/2017 16:51	40.477768	-70.765064	172	SUS S 84 LAST SUS

Some notes from the experiment were included at the end of the log:

- Text typed by GPS user (primarily Wilson and Wan) to identify the event.
- This sometimes includes the station number as well as the description.
- These events include mooring deployment related activities, as well as CSS and SUS events.
- Sometimes a waypoint was recorded before, during and after CSS or SUS stations.
- For example: EOS = end of station
- There are typically multiple CSS or SUS shots fired at every station

## Appendix B. MATLAB Code

*makeSSP.m*

```
% Create and save the sound speed profile for the water column and  
% sediment.
```

```
close all;
```

```
clear;
```

```
% DEPTH
```

```
zwater = 0:0.5:69.5;
```

```
zmud = 70:0.5:75.5;
```

```
zsand = 76:0.5:77.5;
```

```
zdl1 = 78:0.5:84;
```

```
zdl2 = 84.5:0.5:86;
```

```
zbase = 86.5:0.5:300;
```

```
z = [zwater zmud zsand zdl1 zdl2 zbase];
```

```
% SSP
```

```
Cwater = interp1([0 69.5],[1464 1465],z(1:140));
```

```
Cmud = interp1([70 75.5],[1465 1540],z(141:152));
```

```
Csand = 1745*ones(1,length(zsand));
```

```
Cdl1 = 1775*ones(1,length(zdl1));
```

```
Cdl2 = 1625*ones(1,length(zdl2));
```

```
Cbase = 1859*ones(1,length(zbase));
```

```
C = [Cwater Cmud Csand Cdl1 Cdl2 Cbase];
```

```
% Density
```

```
rhewater = 1.03*ones(1,length(zwater));
```

```
rhomud = 1.75*ones(1,length(zmud));
```

```
rhosand = 1.8*ones(1,length(zsand));
```

```
rhodl1 = 1.9*ones(1,length(zdl1));
```

```
rhodl2 = 1.95*ones(1,length(zdl2));
```

```
rhobase = 2*ones(1,length(zbase));
```

```
rho = [rhewater rhomud rhosand rhodl1 rhodl2 rhobase];
```

```
figure;
```

```
subplot(1,2,1)
```

```
plot(C,-z,'b.');
```

```
hold on; plot(C,-z,'r');
```

```
hold on; plot(1400:2000,-70*ones(1,length(1400:2000)),'--k');
```

```
hold on; plot(1400:2000,-76*ones(1,length(1400:2000)),'--k');
```

```
hold on; plot(1400:2000,-78*ones(1,length(1400:2000)),'--k');
```

```
hold on; plot(1400:2000,-84*ones(1,length(1400:2000)),'--k');
```

```
hold on; plot(1400:2000,-86*ones(1,length(1400:2000)),'--k');
```

```
grid on;
```

```
xlabel('Sound Speed (m/s)'); ylabel('Depth Below Water Surface (m)');
```

```
title('Mud Patch Sound Speed Profile');
```

```
ylim([-100 0])

subplot(1,2,2)
plot(rho,-z,'b. '); hold on; plot(rho,-z,'r');
hold on; plot(1:2,-70*ones(1,2),'--k');
hold on; plot(1:2,-76*ones(1,2),'--k');
hold on; plot(1:2,-78*ones(1,2),'--k');
hold on; plot(1:2,-84*ones(1,2),'--k');
hold on; plot(1:2,-86*ones(1,2),'--k');
grid on;
xlabel('\rho (g/cm3)'); title('Mud Patch Density Profile');

ylim([-100 0])
save('mudpatchSSP2.mat','z','C','rho');

% Code originally written by Gopu Potty
% and modified by Kerry Unrein for this study.
```

```

process.m
%% plotting the FFI data
Fidx = [686 766 828 876 910 940 968];
% Corresponds to 32 52 76 102 125 150 178 Hz
ph = 32; % hydrophone (for plot title)
sus = 54; % Station (for plot title)
sus2 = 1; % SUS (for plot title)
load S54_1 % file
fs = sampling frequency
xvar = [1 3]; % x-axis limit on the scalogram
data=S54_1./10^6; % convert microPascal to Pascal
t=(1:length(data(ph,:)).)/fs;
figure; plot(t,data(ph,:));
plot(t-8.5,data(1,:)); hold on
for ii=1:8;
    jj=ii*8;
    offset=(ii-1)+(ii*0.5);
    plot(t-8.9,offset+data(jj,:), 'k', 'linewidth',1.5); hold on;
    xlim([-3 0]);
    ylim([-1 12]);
    set(gca,'YTickLabel',[8 16 24 32 40 48 56 64 ]);
    xlabel('time (s)');
    title(sprintf(' SUS signal S%03d on the FFI array',sus));
end
[DATA1,Fs]=filter_decimate(data(ph,:),fs,4,10,500);
indx_start= 1600 + 1.0e+03 *3.3387;
indx_end= 1.0e+03 * 6.5461 + 100;

DATA1=DATA1(indx_start:indx_end);
[tfr,t,f,wt]=tfrscalo(DATA1',1:1:length(DATA1),25,0.001,0.5,1024,1);
T=t./Fs;F=f*Fs;

figure;
plot(T,DATA1,'k','linewidth',1.5)
xlim(xvar)
xlabel('time (s)'); ylabel(['Acoustic pressure';'(arbitrary units)']);
title(sprintf('SUS %03d (%d): Hydrophone %d',sus,sus2,ph))
set(gcf, 'Units', 'Normalized', 'OuterPosition', [0.1, 0.1, 0.29, 0.22]);

figure % NORMALIZED
max_tfr=max(max(abs(tfr)));
pcolor(T,F,10*log10((abs(tfr))./max_tfr)); shading flat; colormap(jet);
ylim([0 200]);
xlim(xvar);
caxis([-40 0]);
colorbar

```

```

xlabel('time (s)'); ylabel('frequency (Hz)')
title(sprintf('SUS %03d (%d): Hydrophone %d',sus,sus2,ph))

%% loop over different frequencies
for qq = 1:length(Fidx)
    %% plot the amplitude for one frequency indx
    figure; subplot(2,1,1);
    plot(T,abs(wt(Fidx(qq),:)))
    ylabel('amplitude','fontsize',12)
    title(sprintf('SUS %03d (%d) \n Time-Frequency Slice Amplitude at %.1f
        Hz',sus,sus2,F(Fidx(qq))),'fontsize',11)
    xlim(xvar)
    [B,A] = oct3dsgn(F(Fidx(qq)),Fs,3);
    [H,Ffilt] = freqz(B,A,512,Fs);
    data_filtered = filtfilt(B,A,DATA1);
    [X1,X2] = demod(data_filtered,F(Fidx(qq)),Fs,'qam');
    z = X1+X2*1i;

    subplot(2,1,2);
    plot(T,data_filtered,'b'); hold on;
    plot(T,abs(z),'r');
    xlim(xvar)
    xlabel('time (s)','fontsize',12)
    ylabel('amplitude','fontsize',12)
    title(sprintf('Time Series 1/3 Octave Filter \n Centered at %.1f
        Hz',F(Fidx(qq))),'fontsize',11)
    set(gcf, 'Units', 'Normalized', 'OuterPosition', [0, 0.04, 0.2, 0.7]);
    pause
    saveas(gcf,sprintf('S%02d_%03.0fHz_S%03d_%d',ph,F(Fidx(qq)),sus,sus2),'fig')
end

% Code originally written by Gopu Potty
% and modified by Kerry Unrein for this study.

```

*make\_amplitude\_ratios.m*

% This code takes the selected amplitude values by frequency and saves a  
% matrix for use in the GA processing of a single sensor.

close all;

clear;

%% SUS 49\_5 phone 1

% Method 2

md1\_F=[32.1 53.1];

md2\_F=[32.1 53.1 72.4 99.3];

md3\_F=[53.1 72.4 99.3 122.1];

md4\_F=[72.4 99.3 122.1];

md1\_1=[0.1721 0.1405];

md2\_1=[0.3486 0.3484 0.3887 0.3419];

md3\_1=[0.2754 0.36 0.4796 0.2698];

md4\_1=[0.1946 0.2836 0.1885];

ampratio\_12 = ones(2,3);

ampratio\_12(:,1) = md1\_F;

ampratio\_12(:,2) = md1\_1;

ampratio\_12(:,3) = md2\_1(1:2);

save('M2\_S49\_5\_P01\_ampratio\_12.mat','ampratio\_12')

ampratio\_23 = ones(3,3);

ampratio\_23(:,1) = md3\_F(1:3);

ampratio\_23(:,2) = md2\_1(2:end);

ampratio\_23(:,3) = md3\_1(1:3);

save('M2\_S49\_5\_P01\_ampratio\_23.mat','ampratio\_23')

ampratio\_13 = ones(1,3);

ampratio\_13(:,1) = md1\_F(2);

ampratio\_13(:,2) = md1\_1(2);

ampratio\_13(:,3) = md3\_1(1);

save('M2\_S49\_5\_P01\_ampratio\_13.mat','ampratio\_13')

ampratio\_24 = ones(2,3);

ampratio\_24(:,1) = md4\_F(1:2);

ampratio\_24(:,2) = md2\_1(3:end);

ampratio\_24(:,3) = md4\_1(1:2);

save('M2\_S49\_5\_P01\_ampratio\_24.mat','ampratio\_24')

ampratio\_34 = ones(3,3);

ampratio\_34(:,1) = md4\_F;

```
ampratio_34(:,2) = md3_1(2:end);  
ampratio_34(:,3) = md4_1;  
save('M2_S49_5_P01_ampratio_34.mat','ampratio_34')
```

```
% Code originally written by Gopu Potty  
% and modified by Kerry Unrein for this study.
```

```

atten_opt.m
% This program runs the main GA routine 'tbxmpga'
% and specifies options for GA run
% option(1) : output option
% option(14) : No of generations
% option(20) : Population
% option(21) : sub population
%% calls atten_main_5layer.m
%% inputs
% lower and upper bounds of the k and n of the five sediment layers, source
% depth increment and receiver depth increment
% The values defined in atten_main_5layer.m
%% Written by Gopu R Potty (URI); last modified 7/18/2018
%
close all
clear

% GOPTIONSIN
    opt(1) = 2;
    opt(14) = 100;
    opt(20) = 100;
    opt(21) = 1;

%% set up a file to save the individuals and their fitnesses
popSize = 100;
numParam = 13;
populn = [];
prob = [];
save runHist populn prob popSize numParam

tbxmpga('atten_main_5layer',opt,
        [0.0025,1,0.0025,1,0.0025,1,-1,-1.5,0.0025,1,0.0025,1,0.00009],
        [0.09,2,0.09,2,0.09,2,1,1.5,0.09,2,0.09,2,0.00035])

```

```

atten_main_5layer.m
function [f]=atten_main_5layer(x)
% program to calculate the objective function for the GA run
%% called by atten_opt.m/ tbxmpga.m
% calls beta_4layer.m, amp_ratio.m
%%
% Needs to load the modal amplitude data at specified frequencies
% Needs to load (or define) water column sound speed profile
%% Inputs
% x = The trial values for the unknown model parameters generated by GA
%% Output
% f = vector of objective function values for each trail parameter set
%% Written by Gopu R Potty (URI); last modified 7/18/2018
%%

for m=1:length(x(:,1));    % loops through the # of individuals

    xx=x(m,:);

    % assign values for k and n for each layers

    k1=xx(1);
    n1=xx(2);    % vary n from 1 to 2

    k2=xx(3);
    n2=xx(4);    % vary n from 1 to 2

    k3=xx(5);
    n3=xx(6);    % vary n from 1 to 2

    k4=xx(9);
    n4=xx(10);   % vary n from 1 to 2

    k5=xx(11);
    n5=xx(12);   % vary n from 1 to 2

    alpha_basement = xx(13); % alpha value for the basement

    %% %% load water column & sediment ssp (C), density (rho) & depth grid (z)
    load mudpatchSSP2    % loads water column & sediment ssp & depth grid
    %%
    % source and receiver depths with increments
    d_s=18+xx(7);
    d_r=69.5+xx(8);
    h=70;    % water depth

```

```

[dist,phaseangle] = sw_dist([SUSLat phoneLat],[SUSLon phoneLon],'km');

% source-receiver range
r = dist * 1000;

%% SUS49(1)
%% 1. load the modal amplitudes and frequencies - modes 1 and 2
%%
load M2_S49_1_P64_ampratio_12
[diffm]=atten_indiv_12(ampratio_12,k1,n1,k2,n2,k3,n3,k4,n4,k5,n5,alpha_basement,
C,z,rho,d_s,d_r,h,r);
lsum12=sum(diffm.^2); % least squares sum (mode 1/mode 2)
lsum12_S49_1 = lsum12;
clear diffm lsum12

%% 2. load the modal amplitudes and frequencies - modes 3 and 4
%%
load M2_S49_1_P64_ampratio_34
[diffm]=atten_indiv_34(ampratio_34,k1,n1,k2,n2,k3,n3,k4,n4,k5,n5,alpha_basement,
C,z,rho,d_s,d_r,h,r);
lsum34=sum(diffm.^2); % least squares sum (mode 3/ mode 4)
lsum34_S49_1 = lsum34;
clear diffm lsum34

%% 3. load the modal amplitudes and frequencies - modes 2 and 3
%%
load M2_S49_1_P64_ampratio_23
[diffm]=atten_indiv_23(ampratio_23,k1,n1,k2,n2,k3,n3,k4,n4,k5,n5,alpha_basement,
C,z,rho,d_s,d_r,h,r);
lsum23=sum(diffm.^2); % least squares sum
lsum23_S49_1 = lsum23;
clear diffm lsum23

%% 4. load the modal amplitudes and frequencies - modes 1 and 3
%%
load M2_S49_1_P64_ampratio_13
[diffm]=atten_indiv_13(ampratio_13,k1,n1,k2,n2,k3,n3,k4,n4,k5,n5,alpha_basement,
C,z,rho,d_s,d_r,h,r);
lsum13=sum(diffm.^2); % least squares sum (mode 1/mode 3)
lsum13_S49_1 = lsum13;
clear diffm lsum13

%% 5. load the modal amplitudes and frequencies - modes 2 and 4
%%

```

```

load M2_S49_1_P64_ampratio_24
[diffm]=atten_indiv_24(ampratio_24,k1,n1,k2,n2,k3,n3,k4,n4,k5,n5,alpha_basement,
C,z,rho,d_s,d_r,h,r);
lsum24=sum(diffm.^2);      % least squares sum (mode 2/mode 4)
lsum24_S49_1 = lsum24;
clear diffm lsum24

%% SUS49(2)
%% 1. load the modal amplitudes and frequencies - modes 1 and 2
%%
load M2_S49_2_P64_ampratio_12
[diffm]=atten_indiv_12(ampratio_12,k1,n1,k2,n2,k3,n3,k4,n4,k5,n5,alpha_basement,
C,z,rho,d_s,d_r,h,r);
lsum12=sum(diffm.^2);      % least squares sum (mode 1/mode 2)
lsum12_S49_2 = lsum12;
clear diffm lsum12

%% 2. load the modal amplitudes and frequencies - modes 3 and 4
%%
load M2_S49_2_P64_ampratio_34
[diffm]=atten_indiv_34(ampratio_34,k1,n1,k2,n2,k3,n3,k4,n4,k5,n5,alpha_basement,
C,z,rho,d_s,d_r,h,r);
lsum34=sum(diffm.^2);      % least squares sum (mode 3/ mode 4)
lsum34_S49_2 = lsum34;
clear diffm lsum34

%% 3. load the modal amplitudes and frequencies - modes 2 and 3
%%
load M2_S49_2_P64_ampratio_23
[diffm]=atten_indiv_23(ampratio_23,k1,n1,k2,n2,k3,n3,k4,n4,k5,n5,alpha_basement,
C,z,rho,d_s,d_r,h,r);
lsum23=sum(diffm.^2);      % least squares sum
lsum23_S49_2 = lsum23;
clear diffm lsum23

%% 4. load the modal amplitudes and frequencies - modes 1 and 3
%%
load M2_S49_2_P64_ampratio_13
[diffm]=atten_indiv_13(ampratio_13,k1,n1,k2,n2,k3,n3,k4,n4,k5,n5,alpha_basement,
C,z,rho,d_s,d_r,h,r);
lsum13=sum(diffm.^2);      % least squares sum (mode 1/mode 3)
lsum13_S49_2 = lsum13;
clear diffm lsum13

%% 5. load the modal amplitudes and frequencies - modes 2 and 4
%%

```

```

load M2_S49_2_P64_ampratio_24
[diffm]=atten_indiv_24(ampratio_24,k1,n1,k2,n2,k3,n3,k4,n4,k5,n5,alpha_basement,
C,z,rho,d_s,d_r,h,r);
lsum24=sum(diffm.^2);      % least squares sum (mode 2/mode 4)
lsum24_S49_2 = lsum24;
clear diffm lsum24

%% SUS49(3)
%% 1. load the modal amplitudes and frequencies - modes 1 and 2
%%
load M2_S49_3_P64_ampratio_12
[diffm]=atten_indiv_12(ampratio_12,k1,n1,k2,n2,k3,n3,k4,n4,k5,n5,alpha_basement,
C,z,rho,d_s,d_r,h,r);
lsum12=sum(diffm.^2);      % least squares sum (mode 1/mode 2)
lsum12_S49_3 = lsum12;
clear diffm lsum12

%% 2. load the modal amplitudes and frequencies - modes 3 and 4
%%
load M2_S49_3_P64_ampratio_34
[diffm]=atten_indiv_34(ampratio_34,k1,n1,k2,n2,k3,n3,k4,n4,k5,n5,alpha_basement,
C,z,rho,d_s,d_r,h,r);
lsum34=sum(diffm.^2);      % least squares sum (mode 3/ mode 4)
lsum34_S49_3 = lsum34;
clear diffm lsum34

%% 3. load the modal amplitudes and frequencies - modes 2 and 3
%%
load M2_S49_3_P64_ampratio_23
[diffm]=atten_indiv_23(ampratio_23,k1,n1,k2,n2,k3,n3,k4,n4,k5,n5,alpha_basement,
C,z,rho,d_s,d_r,h,r);
lsum23=sum(diffm.^2);      % least squares sum
lsum23_S49_3 = lsum23;
clear diffm lsum23

%% 4. load the modal amplitudes and frequencies - modes 1 and 3
%%
load M2_S49_3_P64_ampratio_13
[diffm]=atten_indiv_13(ampratio_13,k1,n1,k2,n2,k3,n3,k4,n4,k5,n5,alpha_basement,
C,z,rho,d_s,d_r,h,r);
lsum13=sum(diffm.^2);      % least squares sum (mode 1/mode 3)
lsum13_S49_3 = lsum13;
clear diffm lsum13

%% 5. load the modal amplitudes and frequencies - modes 2 and 4
%%

```

```

load M2_S49_3_P64_ampratio_24
[diffm]=atten_indiv_24(ampratio_24,k1,n1,k2,n2,k3,n3,k4,n4,k5,n5,alpha_basement,
C,z,rho,d_s,d_r,h,r);
lsum24=sum(diffm.^2);      % least squares sum (mode 2/mode 4)
lsum24_S49_3 = lsum24;
clear diffm lsum24

%% SUS49(4)
%% 1. load the modal amplitudes and frequencies - modes 1 and 2
%%
load M2_S49_4_P64_ampratio_12
[diffm]=atten_indiv_12(ampratio_12,k1,n1,k2,n2,k3,n3,k4,n4,k5,n5,alpha_basement,
C,z,rho,d_s,d_r,h,r);
lsum12=sum(diffm.^2);      % least squares sum (mode 1/mode 2)
lsum12_S49_4 = lsum12;
clear diffm lsum12

%% 2. load the modal amplitudes and frequencies - modes 3 and 4
%%
load M2_S49_4_P64_ampratio_34
[diffm]=atten_indiv_34(ampratio_34,k1,n1,k2,n2,k3,n3,k4,n4,k5,n5,alpha_basement,
C,z,rho,d_s,d_r,h,r);
lsum34=sum(diffm.^2);      % least squares sum (mode 3/ mode 4)
lsum34_S49_4 = lsum34;
clear diffm lsum34

%% 3. load the modal amplitudes and frequencies - modes 2 and 3
%%
load M2_S49_4_P64_ampratio_23
[diffm]=atten_indiv_23(ampratio_23,k1,n1,k2,n2,k3,n3,k4,n4,k5,n5,alpha_basement,
C,z,rho,d_s,d_r,h,r);
lsum23=sum(diffm.^2);      % least squares sum
lsum23_S49_4 = lsum23;
clear diffm lsum23

%% 4. load the modal amplitudes and frequencies - modes 1 and 3
%%
load M2_S49_4_P64_ampratio_13
[diffm]=atten_indiv_13(ampratio_13,k1,n1,k2,n2,k3,n3,k4,n4,k5,n5,alpha_basement,
C,z,rho,d_s,d_r,h,r);
lsum13=sum(diffm.^2);      % least squares sum (mode 1/mode 3)
lsum13_S49_4 = lsum13;
clear diffm lsum13

%% 5. load the modal amplitudes and frequencies - modes 2 and 4
%%

```

```

load M2_S49_4_P64_ampratio_24
[diffm]=atten_indiv_24(ampratio_24,k1,n1,k2,n2,k3,n3,k4,n4,k5,n5,alpha_basement,
C,z,rho,d_s,d_r,h,r);
lsum24=sum(diffm.^2); % least squares sum (mode 2/mode 4)
lsum24_S49_4 = lsum24;
clear diffm lsum24

%% SUS49(5)
%% 1. load the modal amplitudes and frequencies - modes 1 and 2
%%
load M2_S49_5_P64_ampratio_12
[diffm]=atten_indiv_12(ampratio_12,k1,n1,k2,n2,k3,n3,k4,n4,k5,n5,alpha_basement,
C,z,rho,d_s,d_r,h,r);
lsum12=sum(diffm.^2); % least squares sum (mode 1/mode 2)
lsum12_S49_5 = lsum12;
clear diffm lsum12

%% 2. load the modal amplitudes and frequencies - modes 3 and 4
%%
load M2_S49_5_P64_ampratio_34
[diffm]=atten_indiv_34(ampratio_34,k1,n1,k2,n2,k3,n3,k4,n4,k5,n5,alpha_basement,
C,z,rho,d_s,d_r,h,r);
lsum34=sum(diffm.^2); % least squares sum (mode 3/ mode 4)
lsum34_S49_5 = lsum34;
clear diffm lsum34

%% 3. load the modal amplitudes and frequencies - modes 2 and 3
%%
load M2_S49_5_P64_ampratio_23
[diffm]=atten_indiv_23(ampratio_23,k1,n1,k2,n2,k3,n3,k4,n4,k5,n5,alpha_basement,
C,z,rho,d_s,d_r,h,r);
lsum23=sum(diffm.^2); % least squares sum
lsum23_S49_5 = lsum23;
clear diffm lsum23

%% 4. load the modal amplitudes and frequencies - modes 1 and 3
%%
load M2_S49_5_P64_ampratio_13
[diffm]=atten_indiv_13(ampratio_13,k1,n1,k2,n2,k3,n3,k4,n4,k5,n5,alpha_basement,
C,z,rho,d_s,d_r,h,r);
lsum13=sum(diffm.^2); % least squares sum (mode 1/mode 3)
lsum13_S49_5 = lsum13;
clear diffm lsum13

%% 5. load the modal amplitudes and frequencies - modes 2 and 4
%%

```

```

load M2_S49_5_P64_ampratio_24
[diffm]=atten_indiv_24(ampratio_24,k1,n1,k2,n2,k3,n3,k4,n4,k5,n5,alpha_baseament,
C,z,rho,d_s,d_r,h,r);
lsum24=sum(diffm.^2);    % least squares sum (mode 2/mode 4)
lsum24_S49_5 = lsum24;
clear diffm lsum24
%% cumulative sum of different data sets
ff(m)=sqrt(lsum12_S49_1 + lsum34_S49_1 + lsum23_S49_1 + ...
lsum13_S49_1 + lsum24_S49_1 +...
lsum12_S49_2 + lsum34_S49_2 + lsum23_S49_2 + ...
lsum13_S49_2 + lsum24_S49_2 +...
lsum12_S49_3 + lsum34_S49_3 + lsum23_S49_3 + ...
lsum13_S49_3 + lsum24_S49_3 +...
lsum12_S49_4 + lsum34_S49_4 + lsum23_S49_4 + ...
lsum13_S49_4 + lsum24_S49_4 + ...
lsum12_S49_5 + lsum34_S49_5 + lsum23_S49_5 + ...
lsum13_S49_5 + lsum24_S49_5);    % objective function
end
f=ff';
%% save the 80 best individuals
[y,ii]=sort(f);
prob1=y(1:80);
populn1=x(ii(1:80),:);

load runHist

prob = [prob prob1'];
populn=[populn
populn1];

save runHist populn prob popSize numParam

% Code originally written by Gopu Potty
% and modified by Kerry Unrein for this study.

```

```

atten_indiv_12.m
function [diffm]=atten_indiv_12(ampratio_12,k1,n1,k2,n2,k3,n3,k4,n4,k5,n5,
    alpha_basement,C,z,rho,d_s,d_r,h,r)
%% calculate beta for mode 2
f=ampratio_12(:,1);
NM=2;
%
[beta,Z_s,Z_r,Kappa]=beta_5layer(k1,n1,k2,n2,k3,n3,k4,n4,k5,n5,alpha_basement,f,
    NM,C,z,rho,d_s,d_r,h);
beta_m2=beta;
Z_s_m2=Z_s;
Z_r_m2=Z_r;
Kappa_m2=Kappa;
clear Kappa Z_r Z_s
%
%% calculate beta for mode 1
NM=1;
%
[beta,Z_s,Z_r,Kappa]=beta_5layer(k1,n1,k2,n2,k3,n3,k4,n4,k5,n5,alpha_basement,f,
    NM,C,z,rho,d_s,d_r,h);
beta_m1=beta;
Z_s_m1=Z_s;
Z_r_m1=Z_r;
Kappa_m1=Kappa;
clear Kappa Z_r Z_s
%% calculate the amplitude ratio mode 1/mode 2
[amp_rat12]=amp_ratio(Z_r_m1,Z_r_m2,Z_s_m1,Z_s_m2,Kappa_m1,Kappa_m2,
    beta_m1,beta_m2,r);
% amplitude ratio (data)
amp_rat12_ex=ampratio_12(:,2)./ampratio_12(:,3);
% model-data mis-match
diffm=amp_rat12-amp_rat12_ex';

% Code originally written by Gopu Potty
% and modified by Kerry Unrein for this study.

```

```

atten_indiv_13.m
function [diffm]=atten_indiv_13(ampratio_13,k1,n1,k2,n2,k3,n3,k4,n4,k5,n5,
    alpha_basement,C,z,rho,d_s,d_r,h,r)
f=ampratio_13(:,1);
%% calculate beta for mode 3
NM=3;
%
[beta,Z_s,Z_r,Kappa]=beta_5layer(k1,n1,k2,n2,k3,n3,k4,n4,k5,n5,alpha_basement,f,
    NM,C,z,rho,d_s,d_r,h);
beta_m3=beta;
Z_s_m3=Z_s;
Z_r_m3=Z_r;
Kappa_m3=Kappa;
clear Kappa Z_r Z_s
%
%% calculate beta for mode 1
NM=1;
%
[beta,Z_s,Z_r,Kappa]=beta_5layer(k1,n1,k2,n2,k3,n3,k4,n4,k5,n5,alpha_basement,f,
    NM,C,z,rho,d_s,d_r,h);
beta_m1=beta;
Z_s_m1=Z_s;
Z_r_m1=Z_r;
Kappa_m1=Kappa;
clear Kappa Z_r Z_s
%% calculate the amplitude ratio mode 1/mode 3
[amp_rat13]=amp_ratio(Z_r_m1,Z_r_m3,Z_s_m1,Z_s_m3,Kappa_m1,Kappa_m3,
    beta_m1,beta_m3,r);
% amplitude ratio (data)
amp_rat13_ex=ampratio_13(:,2)./ampratio_13(:,3);
% model-data mis-match
diffm=amp_rat13-amp_rat13_ex';

% Code originally written by Gopu Potty
% and modified by Kerry Unrein for this study.

```

```

atten_indiv_23.m
function [diffm]=atten_indiv_23(ampratio_23,k1,n1,k2,n2,k3,n3,k4,n4,k5,n5,
    alpha_basement,C,z,rho,d_s,d_r,h,r)
f=ampratio_23(:,1);
%% calculate beta for mode 3
NM=3;
%
[beta,Z_s,Z_r,Kappa]=beta_5layer(k1,n1,k2,n2,k3,n3,k4,n4,k5,n5,alpha_basement,f,
    NM,C,z,rho,d_s,d_r,h);
beta_m3=beta;
Z_s_m3=Z_s;
Z_r_m3=Z_r;
Kappa_m3=Kappa;
clear Kappa Z_r Z_s
%
%% calculate beta for mode 2
NM=2;
%
[beta,Z_s,Z_r,Kappa]=beta_5layer(k1,n1,k2,n2,k3,n3,k4,n4,k5,n5,alpha_basement,f,
    NM,C,z,rho,d_s,d_r,h);
beta_m2=beta;
Z_s_m2=Z_s;
Z_r_m2=Z_r;
Kappa_m2=Kappa;
clear Kappa Z_r Z_s
%% calculate the amplitude ratio mode 2/mode 3
[amp_rat23]=amp_ratio(Z_r_m2,Z_r_m3,Z_s_m2,Z_s_m3,Kappa_m2,Kappa_m3,
    beta_m2,beta_m3,r);
% amplitude ratio (data)
amp_rat23_ex=ampratio_23(:,2)./ampratio_23(:,3);
% model-data mis-match
diffm=amp_rat23-amp_rat23_ex';

% Code originally written by Gopu Potty
% and modified by Kerry Unrein for this study.

```

```

atten_indiv_24.m
function [diffm]=atten_indiv_24(ampratio_24,k1,n1,k2,n2,k3,n3,k4,n4,k5,n5,
    alpha_basement,C,z,rho,d_s,d_r,h,r)
f=ampratio_24(:,1);
%% calculate beta for mode 4
NM=4;
%
[beta,Z_s,Z_r,Kappa]=beta_5layer(k1,n1,k2,n2,k3,n3,k4,n4,k5,n5,alpha_basement,f,
    NM,C,z,rho,d_s,d_r,h);
beta_m4=beta;
Z_s_m4=Z_s;
Z_r_m4=Z_r;
Kappa_m4=Kappa;
clear Kappa Z_r Z_s
%
%% calculate beta for mode 2
NM=2;
%
[beta,Z_s,Z_r,Kappa]=beta_5layer(k1,n1,k2,n2,k3,n3,k4,n4,k5,n5,alpha_basement,f,
    NM,C,z,rho,d_s,d_r,h);
beta_m2=beta;
Z_s_m2=Z_s;
Z_r_m2=Z_r;
Kappa_m2=Kappa;
clear Kappa Z_r Z_s
%% calculate the amplitude ratio mode 2/mode 4
[amp_rat24]=amp_ratio(Z_r_m2,Z_r_m4,Z_s_m2,Z_s_m4,Kappa_m2,Kappa_m4,
    beta_m2,beta_m4,r);
% amplitude ratio (data)
amp_rat24_ex=ampratio_24(:,2)./ampratio_24(:,3);
% model-data mis-match
diffm=amp_rat24-amp_rat24_ex';

% Code originally written by Gopu Potty
% and modified by Kerry Unrein for this study.

```

```

atten_indiv_34.m
function [diffm]=atten_indiv_34(ampratio_34,k1,n1,k2,n2,k3,n3,k4,n4,k5,n5,
    alpha_basement,C,z,rho,d_s,d_r,h,r)
f=ampratio_34(:,1);
%% calculate beta for mode 4
NM=4;
%
[beta,Z_s,Z_r,Kappa]=beta_5layer(k1,n1,k2,n2,k3,n3,k4,n4,k5,n5,alpha_basement,f,
    NM,C,z,rho,d_s,d_r,h);
beta_m4=beta;
Z_s_m4=Z_s;
Z_r_m4=Z_r;
Kappa_m4=Kappa;
clear Kappa Z_r Z_s
%
%% calculate beta for mode 3
NM=3;
%
[beta,Z_s,Z_r,Kappa]=beta_5layer(k1,n1,k2,n2,k3,n3,k4,n4,k5,n5,alpha_basement,f,
    NM,C,z,rho,d_s,d_r,h);
beta_m3=beta;
Z_s_m3=Z_s;
Z_r_m3=Z_r;
Kappa_m3=Kappa;
clear Kappa Z_r Z_s
%% calculate the amplitude ratio mode 3/mode 4
[amp_rat34]=amp_ratio(Z_r_m3,Z_r_m4,Z_s_m3,Z_s_m4,Kappa_m3,Kappa_m4,
    beta_m3,beta_m4,r);
amp_rat34_ex=ampratio_34(:,2)./ampratio_34(:,3);
diffm=amp_rat34-amp_rat34_ex';

% Code originally written by Gopu Potty
% and modified by Kerry Unrein for this study.

```

```

beta_5layer.m
function [beta,Z_s,Z_r,Kappa]=beta_5layer(k1,n1,k2,n2,k3,n3,k4,n4,k5,n5,
    alpha_basement,f,NM,C,z,rho,d_s,d_r,h)
% program to calculate the mode attenuation coefficients using attenuation
% profile
% Attenuation profile (alpha(z)) expressed in terms of k*f^n
% Also outputs the eigenvalues and the mode shape values at the source and
% receiver depths
%% called by atten_main_5layer.m
% calls zmode.m
%% inputs:
% k and n for all the layers, depth grid (z), ssp(C), frequency (f) and
% mode number (NM), nominal source and receiver depths (d_s, d_r) and
% density profile (rho)
%% outputs
% modal attenuation coefft (beta), mode shape values at the source and
% receiver depths (Z_s,Z_r) and eigenvalue (Kappa)
%% Written by Gopu R Potty (URI); last modified 7/18/2018
%%
NF=length(f);
nz=length(z);
dz=z(2)-z(1);
Kappa=zeros(NF,1);
Zm=zeros(nz,NF);
%% calculate the eigenvalues and vectors
for nf = 1:NF
    %
    z1=z(2:length(z));c1=C(2:length(C));f1=f(nf);
    [kappa,dummy] = zmode(z1,c1,f1,NM);
    Kappa(nf,:)=kappa(NM);
    Zm(2:nz,nf)=dummy(:,NM);
end
%%
% normalize the mode shapes
%
for fn=1:NF
    for inz=1:nz
        sum_norm(inz,fn)=Zm(inz,fn)^2/(rho(inz)*1.000);
    end
    norm_cnst(fn)=(trapz(sum_norm(1:nz,fn)))*dz; % z(36)=70 m is the bottom
    Psi(:,fn)=Zm(:,fn)./sqrt(norm_cnst(fn));
end
%% calculate the value of the mode shape at source and receiver depths
%
for jj=1:NF
    Z_s(jj,:)=interp1(z,Psi(:,jj),d_s);

```

```

Z_r(jj,:)=interp1(z,Psi(:,jj),d_r);
end

%% Calculate the mode attenuation coefft.
for fn=1:NF
    freq=f(fn)/1000;
    % calculate alpha

    alpha1=k1*freq^n1;
    alpha2=k2*freq^n2;
    alpha3=k3*freq^n3;
    alpha4=k4*freq^n4;
    alpha5=k5*freq^n5;

    % set up the attenuation profile
    % interpolate the attenuation values alpha1 to alpha5 to the entire depth
    alpha_z=interp1([0 70 70.1 76 76.1 78 78.1 84 84.1 86 86.1 100 100.1 z(nz)],...
        [ 0.0000001 0.0000001 alpha1 alpha1 alpha2 alpha2 alpha3 alpha3 alpha4 ...
        alpha4 alpha5 alpha5 alpha_basement alpha_basement],z);

    %% calculate beta

    waven=2*pi*f(fn)./C;

    temp1=(abs(Psi(:,fn))).^2;

    temp2=alpha_z.*temp1';
    temp3=temp2.*waven;

    % z-index corresponding to water depth
    h_indx = interp1(z,1:nz,h);

    temp4=trapz(temp3(h_indx:nz)); % z(36)=70 m is the bottom

    beta(fn)=dz*temp4/Kappa(fn);
end

```

```

amp_ratios.m
function [amp_rat]=
    amp_ratio(Z_r_m1,Z_r_m2,Z_s_m1,Z_s_m2,Kappa_m1,...
        Kappa_m2,beta_m1,beta_m2,r)
%% function to calculate the modal amplitude ratios
% called by atten_main_4layer.m
%% inputs:
% Vaues of mode shapes (for the two modes considered) at the source and
% receiver depths (Z_r_m1,Z_r_m2,Z_s_m1,Z_s_m2), eigenvalues for the two
% modes (Kappa_m1,Kappa_m2), modal attenuation coefficients for the two
% modes (beta_m1,beta_m2), source-receiver range (r)
%% output
% ratio of the modal amplitudes at specified frequencies for the two modes
% considered (amp_rat)
%% Written by Gopu R Potty (URI); last modified 7/18/2018
%%
for jj=1:length(Kappa_m1)
    Kappa_ratio=sqrt(Kappa_m2(jj)/Kappa_m1(jj));
    qnty1=(Z_s_m1(jj))/(Z_s_m2(jj));
    qnty2=(Z_r_m1(jj))/(Z_r_m2(jj));
    qnty4=exp(i*(Kappa_m1(jj)-Kappa_m2(jj))*r);
    qnty3=exp(-r*(beta_m1(jj)-beta_m2(jj)));
    amp_rat(jj)=abs(Kappa_ratio*qnty1*qnty2*qnty3);
end

```

```

posteriori.m
%% Program to read the output of the GA runs and plot the results
% calculates the a posteriori mean and standard deviation
% based on Gerstoft (1994) and Potty et al. (2000)
clear; close all; hold on;
%% PHONE 01 (not shown)
%% PHONE 32 (not shown)
%% PHONE 64
%%%%%%%%%%%%%%%%%%%%%%%%%%%%%%%%%%%%%%%%%%%%%%%%%%%%%%%%%%%%%%%%%%%%%%%%
load runHist_S54_M2_64B
[prob,i]=sort(prob);
N1=50;
T=mean(prob(1:N1));
figure;
populn=populn(i,:);
plot(fliplr(prob),'.')
ylim([0 180])

% 13 parameters; population: 80; generations: 100
N=length(prob);
NumPar=numParam;
%-----
prob=prob./prob(N);    % normalize the cost function
sum1=0.0;
for j=1:N
    sum1=sum1+exp(-prob(j)/T);
end
Sum=sum1;
for j=1:N
    SIGMA(j)=exp(-prob(j)/T)/Sum;
end

% Mean Value
populn=populn';
for k=1:NumPar
    sum1=0.0;
    for j=1:N
        sum1=sum1+(populn(k,j)*SIGMA(j));
    end
    Mean(k)=sum1;
end
% Best Parameter
best=populn(:,1);
%
% Covariance
mm=Mean'*Mean;

```

```

sum2=0.0;
for j=1:N
    mn=populn(:,j)*populn(:,j)*SIGMA(j);
    sum2=sum2+mn;
end
cov=sum2-mm;
% Standard Deviation
std_dv=sqrt(diag(cov));
%-----
%% Attenuation Coefficient Alpha(z)

k=Mean([1 3 5 9 11]);
n=Mean([2 4 6 10 12]);
smean = Mean(7)+18;
rmean = Mean(8)+69.5;
bmean = Mean(13)*8.667;
std_dv_k=std_dv([1 3 5 9 11]);
std_dv_n=std_dv([2 4 6 10 12]);
best_k=best([1 3 5 9 11]);
best_n=best([2 4 6 10 12]);

z=0:1:100;
nz=length(z);
alpha_z=zeros(1,length(z));
freq_kHz=f/1000;
figure(2);
for q = 1:length(freq_kHz)

    %% Mean
    alpha_z(1:6)=k(1)*freq_kHz(q)^n(1);
    alpha_z(7:8)=k(2)*freq_kHz(q)^n(2);
    alpha_z(9:16)=k(3)*freq_kHz(q)^n(3);
    alpha_z(17:18)=k(4)*freq_kHz(q)^n(4);
    alpha_z(19:30)=k(5)*freq_kHz(q)^n(5);
    alpha_z(31:nz)=Mean(13);

    alpha_z=8.667*alpha_z;
    figure(2)
    subplot(1,3,[1 2]); hold on;
    plot(alpha_z,z,'Color',cc(3,:), 'linewidth',3)

    %% Best
    alpha_zb(1:6)=best_k(1)*freq_kHz(q)^best_n(1);
    alpha_zb(7:8)=best_k(2)*freq_kHz(q)^best_n(2);
    alpha_zb(9:16)=best_k(3)*freq_kHz(q)^best_n(3);
    alpha_zb(17:18)=best_k(4)*freq_kHz(q)^best_n(4);

```

```

alpha_zb(19:30)=best_k(5)*freq_kHz(q)^best_n(5);
alpha_zb(31:nz)=best(13);

% alpha in dB/m
alpha_zb=8.667*alpha_zb;
figure(3)
subplot(1,3,[1 2]); hold on;
plot(alpha_zb,z,'Color',cc(3,:), 'linewidth',3)
% Standard Deviation

k1=best_k'+std_dv_k';
n1=best_n'+std_dv_n';
alpha1_z(1:6)=k1(1)*freq_kHz(q)^n1(1);
alpha1_z(7:8)=k1(2)*freq_kHz(q)^n1(2);
alpha1_z(9:16)=k1(3)*freq_kHz(q)^n1(3);
alpha1_z(17:18)=k1(4)*freq_kHz(q)^n1(4);
alpha1_z(19:30)=k1(5)*freq_kHz(q)^n1(5);
alpha1_z(31:nz) = Mean(13)+std_dv(13);
% alpha in dB/m
alpha1_z=8.667*alpha1_z;
alpha1_z=alpha1_z-alpha_z;
figure(2)
subplot(1,3,3); hold on;
plot(abs(alpha1_z),z,'Color',cc(3,:), 'linewidth',3)
figure(3)
subplot(1,3,3); hold on;
plot(abs(alpha1_z),z,'Color',cc(3,:), 'linewidth',3)

end

freq_kHz=(30:10:120)./1000;
alpha1_dBm=8.667*(k(1).*freq_kHz.^n(1));
alpha1b_dBm=8.667*(best_k(1).*freq_kHz.^n(1));
freq_Hz=freq_kHz*1000;

alpha2_dBm=8.667*(k(2).*freq_kHz.^n(2));
alpha2b_dBm=8.667*(best_k(2).*freq_kHz.^n(2));

alpha3_dBm=8.667*(k(3).*freq_kHz.^n(3));
alpha3b_dBm=8.667*(best_k(3).*freq_kHz.^n(3));

alpha4_dBm=8.667*(k(4).*freq_kHz.^n(4));
alpha4b_dBm=8.667*(best_k(4).*freq_kHz.^n(4));

alpha5_dBm=8.667*(k(5).*freq_kHz.^n(5));
alpha5b_dBm=8.667*(best_k(5).*freq_kHz.^n(5));

```

```

figure(2); subplot(1,3,[1 2]);
xlabel('Attenuation \alpha(z) (dB/m)')
ylabel('depth below seafloor (m)')
title('Posteriori Mean Attenuation Coefficient \alpha(z) (dB/m) at 50 hertz'); grid on;
legend('Phone 1','Phone 32','Phone 64','location','northeast');
ylim([0 30])
xlim([0 0.03])
axis ij
subplot(1,3,3);
ylim([0 30])
xlim([0 0.003])
ax.XTickLabel = {'0','0.001','0.002','0.003'};
set(gca,'xticklabel',ax.XTickLabel)
axis ij
xlabel('Standard Deviation (dB/m)')
ylabel('depth below seafloor (m)')
title('Standard Deviation (dB/m)'); grid on;
set(gcf, 'Units', 'Normalized', 'OuterPosition', [0, 0.04, 0.5, 0.65])

figure(3); subplot(1,3,[1 2]);
xlabel('Attenuation \alpha(z) (dB/m)')
ylabel('depth below seafloor (m)')
title('Best Attenuation Coefficients \alpha(z) (dB/m) at 50 hertz'); grid on;
legend('Phone 1','Phone 32','Phone 64','location','northeast');
ylim([0 30])
xlim([0 0.03])
subplot(1,3,3);
ylim([0 30])
xlim([0 0.003])
ax.XTickLabel = {'0','0.001','0.002','0.003'};
set(gca,'xticklabel',ax.XTickLabel)
xlabel('Standard Deviation (dB/m)')
axis ij
ylabel('depth below seafloor (m)')
title('Standard Deviation (dB/m)'); grid on;
set(gcf, 'Units', 'Normalized', 'OuterPosition', [0, 0.04, 0.5, 0.65]);

```

% Code originally written by Gopu Potty  
% and modified by Kerry Unrein for this study.

```

calcArrTime.m
clear
close all
%% Spectrogram Hydrophone Channel 1
%% plot data and TFR
%% if time series of the SUS is available, input here as DATA1
% Potty et al., 2003;
indx_start = 6e4;
indx_end = 6.8e4;
load S49_1
F=0.1:1:250;
sample_freq = sample frequency
DATA1=S49_1(1,indx_start:indx_end);
figure; plot(DATA1)
[B1,F1,T1] = spectrogram(DATA1,1024,750,F,sample_freq);
figure(1)
pcolor(T1,F1,20*log10(abs(B1)));shading flat; colormap(jet)
axis xy
ylabel('Freq, Hz');
xlabel('Time, seconds');
%%
[DATA1,Fs]=filter_decimate(DATA1,sample_freq,9,10,500);
[tfr,t,f,wt]=tfrscal0(DATA1',1:1:length(DATA1),25,0.001,0.3,512,1);
T=t./Fs;F=f*Fs;
figure(2)
max_tfr=max(max(abs(tfr)));
pcolor(T,F,10*log10((abs(tfr))./max_tfr));shading flat;colormap(jet)
caxis([-70 0])
colorbar
xlabel('time (s)'); ylabel('frequency (Hz)')
title('Station 49 SUS #1: Hydrophone 1')
%%
[xm1,ym1] = ginput
[xm2,ym2] = ginput
[xm3,ym3] = ginput
[xm4,ym4] = ginput
load arrTime_49_1B
figure(2); hold on
plot(arrTime_m1,freq_m1,'*w')
plot(arrTime_m2,freq_m2,'*w')
plot(arrTime_m3,freq_m3,'*w')
plot(arrTime_m4,freq_m4,'*w')

```

```

calcRange.m
%% Program to calculate range from travel time difference
% Potty et al., 2003; Eqns:5,6, and 7
clear
close all
%% load the arrival time data (frequency and arrival times); 4 modes
load arrTime_49_1
%% load water column & sediment ssp (C), density (rho) & depth grid (z)
z1=0:1:700;
nz=length(z1);
%
load mudpatchSSP2      % loads water column & sediment ssp & depth grid
C1=interp1([z 700],[C C(length(z))],z1);
rho1=interp1([z 700],[rho rho(length(z))],z);
C=C1;
rho=rho1;
z=z1;
clear z1 C1 rho1
%
freq=5:0.1:125;
NM=4;
%% Calculate group velocity
[vg0]=PERTINV_SCALE(NM,C,freq,z);
%% mode 1 ; equation 5
deltaT1=arrTime_m1(2:length(arrTime_m1))-arrTime_m1(1);
vg0_model1=interp1(freq,vg0(1,:),freq_m1);
K_t1=(1./vg0_model1(2:length(arrTime_m1)))-(1./vg0_model1(1));
% mode 2; equation 5
deltaT2=arrTime_m2(2:length(arrTime_m2))-arrTime_m2(1);
vg0_model2=interp1(freq,vg0(2,:),freq_m2);
K_t2=(1./vg0_model2(2:length(arrTime_m2)))-(1./vg0_model2(1));
% mode 3; equation 5
deltaT3=arrTime_m3(2:length(arrTime_m3))-arrTime_m3(1);
vg0_model3=interp1(freq,vg0(3,:),freq_m3);
K_t3=(1./vg0_model3(2:length(arrTime_m3)))-(1./vg0_model3(1));
% mode 4; equation 5
deltaT4=arrTime_m4(2:length(arrTime_m4))-arrTime_m4(1);
vg0_model4=interp1(freq,vg0(4,:),freq_m4);
K_t4=(1./vg0_model4(2:length(arrTime_m4)))-(1./vg0_model4(1));
%%
plot(K_t1,deltaT1,'*',K_t3,deltaT3,'k*',K_t4,deltaT4,'g*');
x=[K_t1' K_t3' K_t4'];
y=[deltaT1' deltaT3' deltaT4'];
%% Equation 6; mode 1 and 2
f12=30:5:55;
arrTime_m1_interp=interp1(freq_m1,arrTime_m1,f12);

```

```

arrTime_m2_interp=interp1(freq_m2,arrTime_m2,f12);
deltaT12=arrTime_m1_interp-arrTime_m2_interp;
vg0_model1=interp1(freq,vg0(1,:),f12);
vg0_model2=interp1(freq,vg0(2,:),f12);
K_t12=(1./vg0_model1)-(1./vg0_model2);
hold on; plot(K_t12,deltaT12,'r+');
x=[x K_t12];
y=[y deltaT12];
%% Equation 6; mode 2 and 3
f23=50:5:80;
arrTime_m2_interp=interp1(freq_m2,arrTime_m2,f23);
arrTime_m3_interp=interp1(freq_m3,arrTime_m3,f23);
deltaT23=arrTime_m2_interp-arrTime_m3_interp;
vg0_model2=interp1(freq,vg0(2,:),f23);
vg0_model3=interp1(freq,vg0(3,:),f23);
K_t23=(1./vg0_model2)-(1./vg0_model3);
hold on;plot(K_t23,deltaT23,'g+')
x=[x K_t23];
y=[y deltaT23];
%% Equation 6; mode 2 and 4
f24=65:5:80;
arrTime_m2_interp=interp1(freq_m2,arrTime_m2,f24);
arrTime_m4_interp=interp1(freq_m4,arrTime_m4,f24);
deltaT24=arrTime_m2_interp-arrTime_m4_interp;
vg0_model2=interp1(freq,vg0(2,:),f24);
vg0_model4=interp1(freq,vg0(4,:),f24);
K_t24=(1./vg0_model2)-(1./vg0_model4);
hold on; plot(K_t24,deltaT24,'k+')
x=[x K_t24];
y=[y deltaT24];
%% Equation 6; mode 1 and 4
f14=75:5:90;
arrTime_m1_interp=interp1(freq_m1,arrTime_m1,f14);
arrTime_m4_interp=interp1(freq_m4,arrTime_m4,f14);
deltaT14=arrTime_m1_interp-arrTime_m4_interp;
vg0_model1=interp1(freq,vg0(1,:),f14);
vg0_model4=interp1(freq,vg0(4,:),f14);
K_t14=(1./vg0_model1)-(1./vg0_model4);
hold on;plot(K_t14,deltaT14,'r+')
x=[x K_t14];
y=[y deltaT14];
%% Equation 6; mode 3 and 4
f34=70:5:100;
arrTime_m3_interp=interp1(freq_m3,arrTime_m3,f34);
arrTime_m4_interp=interp1(freq_m4,arrTime_m4,f34);
deltaT34=arrTime_m3_interp-arrTime_m4_interp;

```

```

vg0_model3=interp1(freq,vg0(3,:),f34);
vg0_model4=interp1(freq,vg0(4,:),f34);
K_t34=(1./vg0_model3)-(1./vg0_model4);
hold on; plot(K_t34,deltaT34,'b+')
x=[x K_t34];
y=[y deltaT34];
%% Equation 6; mode 1 and 3
f13=[45 50];
arrTime_m1_interp=interp1(freq_m1,arrTime_m1,f13);
arrTime_m3_interp=interp1(freq_m3,arrTime_m3,f13);
deltaT13=arrTime_m1_interp-arrTime_m3_interp;
vg0_model1=interp1(freq,vg0(1,:),f13);
vg0_model3=interp1(freq,vg0(3,:),f13);
K_t13=(1./vg0_model1)-(1./vg0_model3);
hold on; plot(K_t13,deltaT13,'r+')
x=[x K_t13];
y=[y deltaT13];
figure(2);plot(x,y,'k*')
%% fit a line
[rnum,cnum] = find(~isnan(y));
xx = x(cnum);
yy = y(cnum);
[rnum2,cnum2] = find(~isnan(xx));
xxx = xx(cnum2);
yyy = yy(cnum2);
p = polyfit(xxx,yyy,1) % p(1) is slope and p(2) is intercept
y_predict=(p(1).*xxx)+p(2); % generate y using y=max+c
hold on
plot(xxx,y_predict,'k','linewidth',4) % plot the line
disp(num2str(p(1)/1000))
xlabel('Kt(f) Theoretical Group Slowness')
ylabel('DeltaT(f) Experimental Travel Time Difference')
grid on;
xlim([-5e-5 0])
ax.XTickLabel = {'-0.00005','-0.000045','-0.00004','-0.000035',...
'-0.00003','-0.000025','-0.00002','-0.000015','-0.00001','0.00000'};
set(gca,'xticklabel',ax.XTickLabel)

```

% Code originally written by Gopu Potty  
% and modified by Kerry Unrein for this study.

```
make_arrTime.m
```

```
close all
```

```
clear
```

```
arrTime_m1 = [0.6772; 0.6515; 0.6325; 0.5609; 0.5351];  
freq_m1 = [23.0678; 25.5436; 29.1621; 49.3494; 71.4411];  
[v1,c1]=unique(freq_m1);  
freq_m1 = freq_m1(c1);  
arrTime_m1 = arrTime_m1(c1);
```

```
arrTime_m2 = [1.0498; 1.0442; 1.0375; 1.0375; 0.9950; 0.9558; 0.9077;...  
0.7891; 0.7891; 0.7668; 0.6739; 0.6504; 0.5676; 0.5374];  
freq_m2 = [30.1143; 32.0188; 33.7328; 33.7328; 38.3035; 39.4462; ...  
40.5889; 48.3971; 48.3971; 50.3016; 68.9653; 72.3933; 97.3417; 117.9099];  
[v2,c2]=unique(freq_m2);  
freq_m2 = freq_m2(c2);  
arrTime_m2 = arrTime_m2(c2);
```

```
arrTime_m3 = [1.0733; 1.0621; 0.9100; 0.8887; 0.8574; 0.7287; 0.7175;...  
0.6392; 0.5889];  
freq_m3 = [51.2538; 52.0156; 68.7748; 70.2984; 72.5838; 95.4373; ...  
97.5322; 117.5290; 135.2404];  
[v3,c3]=unique(freq_m3);  
freq_m3 = freq_m3(c3);  
arrTime_m3 = arrTime_m3(c3);
```

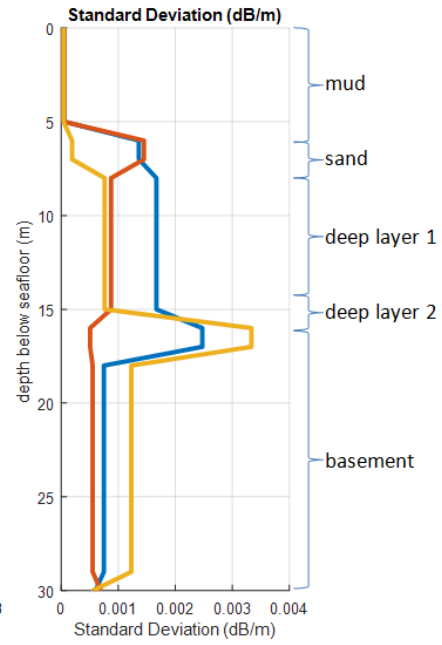
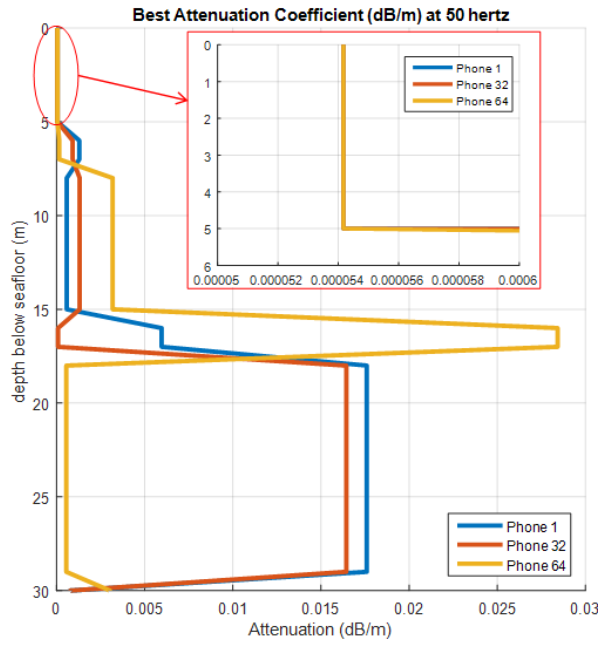
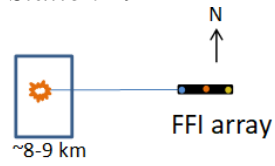
```
arrTime_m4 = [1.0868; 1.0689; 0.9111; 0.8898; 0.7645; 0.6784; 0.6784];  
freq_m4 = [70.6793; 72.3933; 94.6755; 98.6748; 117.7194; 140.5729; 140.5729];  
[v4,c4]=unique(freq_m4);  
freq_m4 = freq_m4(c4);  
arrTime_m4 = arrTime_m4(c4);
```

```
save('arrTime_49_1B','arrTime_m1','arrTime_m2','arrTime_m3','arrTime_m4',...  
'freq_m1','freq_m2','freq_m3','freq_m4')
```

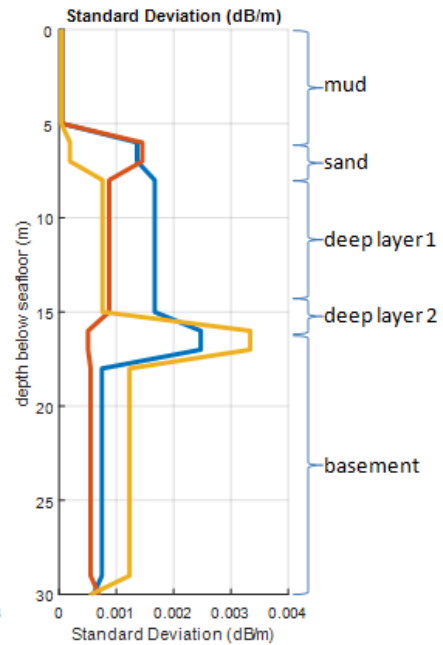
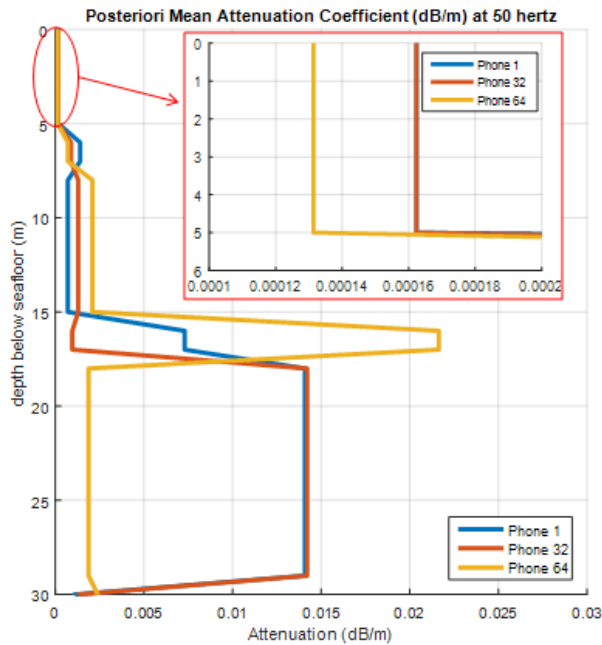
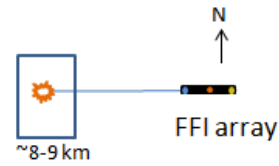
```
% Code originally written by Gopu Potty  
% and modified by Kerry Unrein for this study.
```

Appendix C. Attenuation Coefficient by Depth for Station 49

Best Attenuation Coefficients for Station 49  
Phones 1, 32, and 64 SUS #1-5

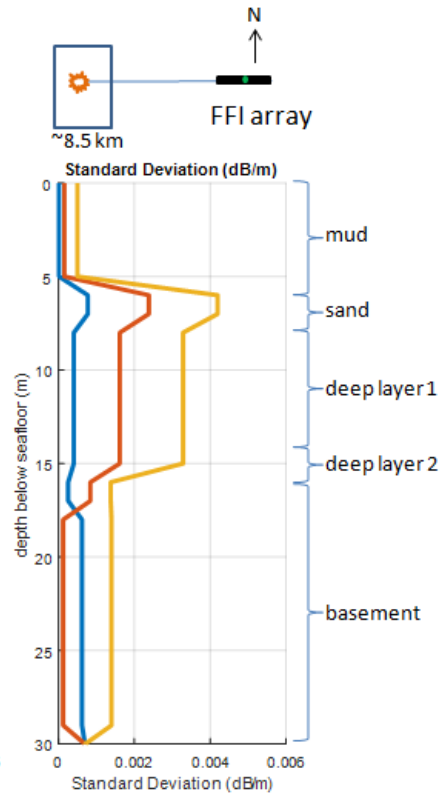
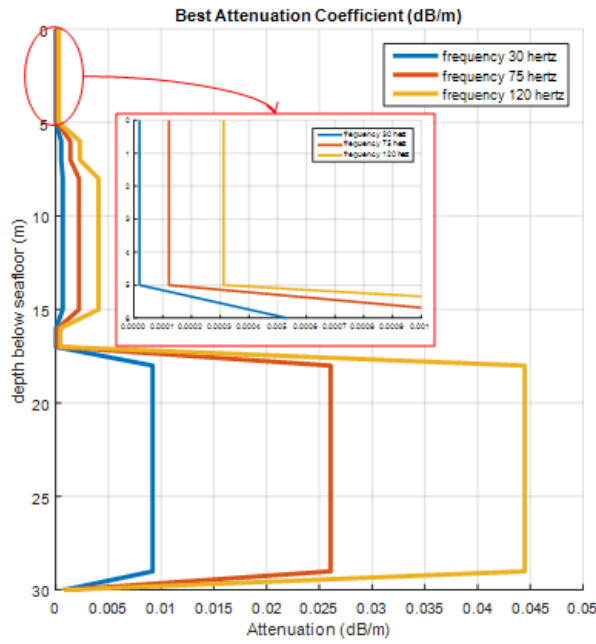


Posteriori Mean Attenuation Coefficients for  
Station 49 Phones 1, 32, and 64 SUS #1-5

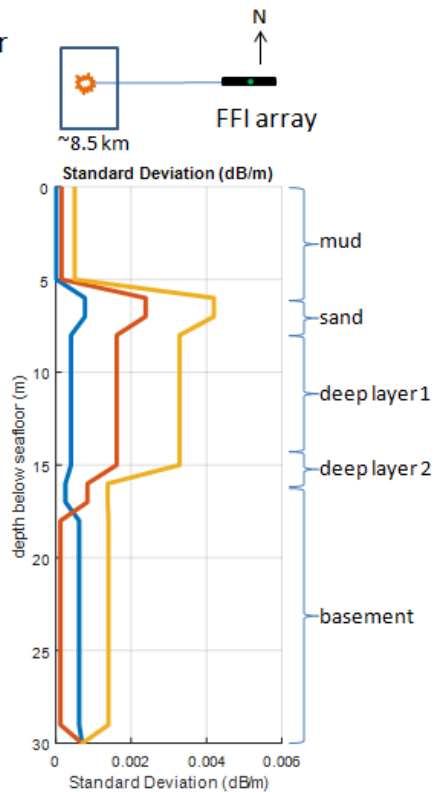
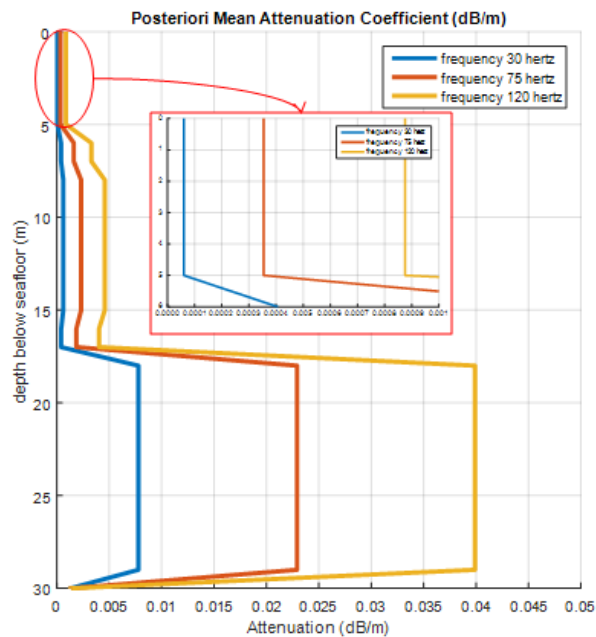


Attenuation Coefficient Frequency Dependence for Station 49

Best Attenuation Coefficients for Station 49 Phone 32 SUS #1-5  
Frequencies 30, 75, and 120 hertz



Posteriori Mean Attenuation Coefficients for Station 49 Phone 32 SUS #1-5  
Frequencies 30, 75, and 120 hertz



## BIBLIOGRAPHY

- Ainslie, Michael and James McColm. "A simplified formula for viscous and chemical absorption in sea water." *Journal of the Acoustical Society of America*, vol. 103, no. 3, pp. 1671-1672, 1998.
- Badiey, Mohsen et al. "From geology to geoacoustics – Evaluation of Biot-Stoll sound speed and attenuation for shallow water acoustics." *Journal of the Acoustical Society of America*, vol. 103, no. 1, pp. 309-320, 1998.
- Bonnel, Julien et al. "Geoacoustic inversion on the New England Mudpatch using warping and dispersion curves of higher order modes." *The Journal of the Acoustical Society of America*, vol. 143, no. 5, pp. 405-411, 2018.
- Bonnel, Julien et al. "Modal depth function estimation using time-frequency analysis." *The Journal of the Acoustical Society of America*, vol. 130, no. 1, pp. 61-71, 2011.
- Buchanan, James. *An Assessment of the Biot-Stoll Model of a Poroelastic Seabed*. Naval Research Laboratory. 5 August 2005.
- Buckingham, Michael J. "Theory of acoustic attenuation, dispersion, and pulse propagation in unconsolidated granular materials including marine sediments." *The Journal of the Acoustical Society of America*, vol. 102, no. 5, pp. 2579-2596, 1997.
- Engineering ToolBox, (2014). *Sea Water – Attenuation of Sound*.  
[www.engineeringtoolbox.com/sea-water-sound-attenuation-d\\_1889.html](http://www.engineeringtoolbox.com/sea-water-sound-attenuation-d_1889.html)  
Accessed 15 Oct 2018.
- Frisk, George. *Ocean and Seabed Acoustics: A Theory of Wave Propagation*. 1<sup>st</sup> ed., Prentice-Hall, Inc. 1994.
- Gerstoft, Peter. "Inversion of seismoacoustic data using genetic algorithms and a *posteriori* probability distributions." *The Journal of the Acoustical Society of America*, vol. 95, no. 2, pp. 770-782, 1994.
- Goff, John et al. "Stratigraphic analysis of a sediment pond within the southern New England Mud Patch: New Constraints from high-resolution chirp acoustic reflection data," *Marine Geology*, 2018.
- Hamilton, Edwin. "Geoacoustic modeling of the sea floor." *The Journal of the Acoustical Society of America*, vol. 68, no. 5, pp. 1313-1340, 1980.
- Jensen, Finn et al. *Computational Ocean Acoustics*. 1<sup>st</sup> ed., American Institute of

Physics, 1994.

Knobles, David P. et al. "Maximum entropy derived statistics of sound speed structure in a fine-grained sediment inferred from sparse broadband acoustic measurements on the New England continental shelf." *IEEE Journal of Oceanic Engineering*, 2019 (accepted for publication).

MATLAB Central. [mathworks.com/matlabcentral/](http://mathworks.com/matlabcentral/). Accessed 10 Mar. 2018.

Menke, William. *Geophysical Data Analysis: Discrete Inverse Theory*. 3<sup>rd</sup> ed., Elsevier, 2012.

Miller, James H. "Estimation of sea surface wave spectra using acoustic tomography." 1987. Massachusetts Institute of Technology and the Woods Hole Oceanographic Institution.

Morgan, Phil and Steve Rintoul. *swdist.m*. CSIRO. 1992. MATLAB function.

National Data Buoy Center. *Buoy 44097*. [www.ndbc.noaa.gov/](http://www.ndbc.noaa.gov/) Accessed 30 July 2018.

*Ocean Acoustics Library*. Scripps Institution UCSD. [oalib.hlsresearch.com/Other/demo](http://oalib.hlsresearch.com/Other/demo). Accessed 6 Oct. 2018.

Pierce, Allan et al. "Analytical discussion of past measurements of acoustic attenuation in mud sediments and of possible future experimental approaches." *The Journal of the Acoustical Society of America*, vol. 138, p. 1933, 2015.

Pohlheim, Hartmut. *GEATbx: Genetic and Evolutionary Algorithm Toolbox for use with MATLAB Documentation*. Version 3.80. Dec 2006.

Porter, Michael. *Ocean Acoustic Modeling in MATLAB*. Science Applications International Corp.

Porter, Michael. *The KRAKEN Normal Mode Program*. Naval Research Laboratory. 22 May 1992.

Potty, Gopu. "Broadband Nonlinear Inversion for Geoacoustic Parameters in Shallow Water." 2000. The University of Rhode Island.

Potty, Gopu. "Vibrating String." OCE 571, 26 May 2015, The University of Rhode Island, Narragansett, RI. Lecture.

Potty, Gopu et al. "Characterization of bottom parameters in the New England Mud Patch using geophone and hydrophone measurements." *The Journal of the Acoustical Society of America*, vol. 144, p. 1973, 2018.

- Potty, Gopu et al. "Inversion for sediment Geoacoustic properties at the New England Bight." *The Journal of the Acoustical Society of America*, vol. 114, no. 4, pp. 1874-1887, 2003.
- Potty, Gopu et al. "Tomographic mapping of sediments in shallow water." *Journal of the Acoustical Society of America*, vol. 108, no. 3, pp. 973-986, 2000.
- Rajan, Subramaniam et al. "On the determination of modal attenuation coefficients and compressional wave attenuation profiles in a range dependent environment in Nantucket sound." *IEEE Journal of Oceanic Engineering*, vol. 17, no. 1, pp. 118-127, 1992.
- Rajan, Subramaniam et al. "Perturbative inversion methods for obtaining bottom geoacoustic parameters in shallow water." *The Journal of the Acoustical Society of America*, vol. 82, no. 3, pp. 998-1017, 1987.
- Stoll, Robert. "Marine sediment acoustics." *The Journal of the Acoustical Society of America*, vol. 77, no. 5, pp. 1789-1799, 1985.
- Office of Naval Research. "*SUS Source Level Committee Report. Long Range Acoustic Propagation Project.*" November 1975.
- Tang, K.S et al. "Genetic Algorithms and their Applications." *IEEE Signal Processing Magazine*, vol. 13, no. 6, pp. 22-37, 1996.
- Tindle, C.T. "Attenuation parameters from normal mode measurements." *The Journal of the Acoustical Society of America*, vol. 71, no. 5, pp. 1145-1148, 1982.
- Urick, Robert J. *Principles of Underwater Sound*. 3<sup>rd</sup> ed., McGraw-Hill, Inc., 1983.
- Wan, Lin et al. "Low-frequency sound speed and attenuation in sandy seabottom from long-range broadband acoustic measurements." *The Journal of the Acoustical Society of America*, vol. 128, no. 2, pp. 578-589, 2010.
- Zhou, Ji-Xun et al. "Low-frequency geoacoustic model for the effective properties of sandy seabottoms." *The Journal of the Acoustical Society of America*, vol. 125, no. 5, pp. 2847-2866, 2009.
- Zhou, Ji-Xun et al. "Geoacoustic parameters in a stratified sea bottom from shallow water acoustic propagation." *The Journal of the Acoustical Society of America*, vol. 82, no. 6, pp. 2068-2074, 1987.